The intervertebral disc contains intrinsic circadian clocks that are regulated by age and cytokines and linked to degeneration

DOI:
10.1136/annrheumdis-2016-209428

Document Version
Accepted author manuscript

Annals of the
RHEUMATIC DISEASES
The Eular Journal

The intervertebral disc contains intrinsic circadian clocks that are regulated by age and cytokines and linked to degeneration

Journal:	*Annals of the Rheumatic Diseases*
Manuscript ID	annrheumdis-2016-209428.R1
Article Type:	Extended report
Date Submitted by the Author:	06-Jun-2016
Complete List of Authors:	Dudek, Michal; University of Manchester Yang, Nan; University of Manchester Pathiranage, Dharshika; University of Manchester Williams, Jack; University of Manchester Borysiewicz, Elzbieta; University of Manchester Wang, Ping; University of Manchester Adamson, Antony; University of Manchester Li, Jian; University of Manchester Bateman, John; 2, Murdoch Childrens Research Institute White, Michael; University of Manchester Boot-handford, Ray; University of Manchester Hoyland, Judith; University of Manchester, Centre for Tissue Injury and Repair, Faculty of Medical and Human Sciences; University of Manchester, NIHR Manchester Musculoskeletal Biomedical Research Unit, Manchester Academic Health Science Centre Meng, Qing-Jun; University of Manchester,
Keywords:	Low Back Pain, Cytokines, Arthritis, Chondrocytes

Note: The following files were submitted by the author for peer review, but cannot be converted to PDF. You must view these files (e.g. movies) online.

Supplementary video 1.avi
Supplementary Video 2.avi
Supplementary video 3.avi

The intervertebral disc contains intrinsic circadian clocks that are regulated by age and cytokines and linked to degeneration

Michal Dudek[1], Nan Yang[1], Jayalath PD Ruckshanthi[1], Jack Williams[1], Elzbieta Borysiewicz[1], Ping Wang[1], Antony Adamson[1], Jian Li[1], John F. Bateman[2], Michael R. White[1], Raymond P. Boot-Handford[3], Judith A Hoyland[4,5]*, Qing-Jun Meng[1,3]*

[1]Faculty of Life Sciences, University of Manchester, A.V.Hill Building, Oxford Road, Manchester, M13 9PT, UK.

[2]Murdoch Childrens Research Institute, Parkville, Victoria 3052, Australia.

[3]Wellcome Trust Centre for Cell Matrix Research, University of Manchester, Oxford Road, Manchester, M13 9PT, UK.

[4]Centre for Tissue Injury and Repair, Faculty of Medical and Human Sciences, University of Manchester, Stopford Building, Oxford Road, Manchester, M13 9PT.

[5]NIHR Manchester Musculoskeletal Biomedical Research Unit, Manchester Academic Health Science Centre, Manchester, UK

*Corresponding authors:

Dr. Qing-Jun Meng, Faculty of Life Sciences, University of Manchester, A.V.Hill Building, Oxford Road, Manchester, M13 9PT, UK. Email: qing-jun.meng@manchester.ac.uk Tel: +44 161 3068912.

Prof. Judith A Hoyland, Centre for Tissue Injury and Repair, Faculty of Medical and Human Sciences, University of Manchester, Stopford Building, Oxford Road, Manchester, M13 9PT. Email: judith.a.hoyland@manchester.ac.uk Tel: +44 161 2755425.

Running Title: IVD clock and degeneration

Key words: circadian clock, intervertebral disc, cytokine, ageing, *Bmal1*

Abstract

Objectives: The circadian clocks are internal timing mechanisms that drive ~24 hr rhythms in a tissue-specific manner. Many aspects of the physiology of the intervertebral disc (IVD) show clear diurnal rhythms. However, it is unknown whether IVD tissue contains functional circadian clocks and if so, how their dysregulation is implicated in IVD degeneration.

Methods: Clock gene dynamics in *ex vivo* IVD explants (from PER2::LUC reporter mice) and human disc cells (transduced with lentivirus containing *Per2*::luc reporters) were monitored in real-time by bioluminescence photon counting and imaging. Temporal gene expression changes were studied by RNAseq and qRT-PCR. IVD pathology was evaluated by histology in a mouse model with tissue-specific deletion of the core clock gene *Bmal1*.

Results: Here we show the existence of the circadian rhythm in mouse IVD tissue and human disc cells. This rhythm is dampened with ageing in mice and can be abolished by treatment with IL-1β but not TNFα. Time series RNAseq revealed 607 genes with 24 hr patterns of expression representing several essential pathways in IVD physiology. Mice with conditional knockout of *Bmal1* in their disc cells demonstrated age-related degeneration of IVDs.

Conclusions: We have established autonomous circadian clocks in mouse and human IVD cells which respond to age and cytokines, and control key pathways involved in the homeostasis of IVDs. Genetic disruption to the mouse IVD molecular clock predispose to IVD degeneration. These results support the concept that disruptions to circadian rhythms may be a risk factor for degenerative IVD disease and low back pain.

Introduction

The circadian clocks are internal timing mechanisms which drive ~24 hr rhythms in physiology and behaviour. In mammals, the central pacemaker Suprachiasmatic Nuclei (SCN) in the hypothalamus synchronizes peripheral clocks in most major body organs.[1-3] Circadian rhythms coordinate tissue-specific physiology with light/darkness, rest/activity feeding cycles and body temperature fluctuations.[1 4] Disruptions to circadian rhythms (during ageing or in shift workers) have been linked to increased risk of diseases (e.g. obesity, diabetes, cardiovascular disease, and osteoarthritis.[5 6] At the molecular level, the circadian clock consists of a network of transcriptional activators (*Clock*, *Bmal1*) and repressors (*Per1/2* and *Cry1/2*) organized in a negative feedback loop.[6] This core oscillator generates 24 hour rhythms in the expression of not only its core components but also a myriad of clock controlled genes (CCGs). Depending on the tissue, expression of 3-16% of the whole transcriptome exhibits a circadian rhythm.[7]

The spine is comprised of bony vertebral bodies alternating with fibro-cartilagenous intervertebral discs (IVD). IVD degeneration is among the most prevalent musculoskeletal disorders affecting one in five people under 60 and more than half of the people above 60 years of age.[8] Low back pain, which is often associated with IVD degeneration, is the number one cause of Years Lived with Disability in the developed countries.[9] Existing evidence suggests that the IVD is a highly rhythmic tissue, experiencing a diurnal cycle of higher loading (activity phase),[10 11] followed by a period of low-load recovery (resting phase). Under high load the pressurized interstitial fluid flows to regions of lower pressure through the outer annulus fibrosus (AF) and the cartilaginous end plate (CEP), resulting in decreased disc height, AF outward bulging and an increase in osmolarity of the central gelatinous nucleus pulposus (NP). During the recovery period, the process is reversed by high osmotic pressure inside the disc causing fluid flow to the NP.[12] Exchange of nutrients/metabolites that occurs with fluid flow during this cycle maintains disc cell homeostasis.[13]

Consistent with the rhythmic nature of IVD tissue, shift work (a factor known to disrupt circadian rhythms) was reported to be associated with higher risk of LBP and IVD degeneration.[14-18] We have previously shown that environmental disruption of circadian rhythm in mice, when combined with high fat diet, leads to degeneration of the lumbar IVD tissue in mice.[19] More recently, changes in the expression of circadian clock genes have been identified in rat IVD tissues following passive smoking (a risk factor for LBP).[20] However, no studies have examined whether IVD cells express intrinsic circadian clocks, how these IVD clocks are regulated, what their targets are, and whether genetic disruption to the IVD clock impact on tissue homeostasis and susceptibility to degeneration.

In this study, we systemically characterized the molecular circadian clock mechanisms in mouse and human IVD tissue/cells. Moreover, by generating a tissue-specific *Bmal1* KO mouse model, our study provides the first genetic evidence linking a core clock factor to IVD degeneration.

Results

Intervertebral disc possesses a functional, temperature entrainable circadian clock

To test whether the IVD contains a molecular circadian clock capable of driving circadian rhythm of gene expression we monitored the dynamics of PER2::Luc protein in IVD explant cultures isolated from PER2::Luc reporter mice.[21] Real-time bioluminescence photon counting demonstrated robust circadian rhythm of PER2::Luc activity which lasted for more than 5 days, with a period of 23.93 +/- 0.10 hrs (mean +/- SEM, n=6, Fig. 1A). As the IVD comprises two distinct cell types, the NP and AF cells, we wanted to know if both regions exhibit circadian rhythms. Live imaging of the mouse IVD explants using high sensitivity EM-CCD camera revealed rhythmic PER2::Luc signals from both AF and NP cells (see Supplementary videos 1-3). To extend these studies to humans, primary human NP cells were transiently transfected with a vector carrying the luciferase gene under the control of the *Per2* promoter. This approach revealed cell autonomous circadian oscillations of *Per2::luc* expression, indicating the operation of a functional clock machinery in these human disc cells (Fig. 1B). IHC staining of human NP tissue sections using antibodies against BMAL1 and CLOCK confirmed presence of these essential circadian clock components in human discs (Fig. 1C).

One of the key properties of a peripheral circadian clock is their ability to respond to time cues that are controlled by the SCN clock, such as hormones or changes in body temperature. Since the IVDs are not vascularised or innervated (except in pathological conditions)[22], we hypothesised that daily body temperature oscillations may be a mechanism of clock entrainment for IVDs. To test this, IVD explants from the same mouse were placed in different incubators programmed to have oppositely phased cyclic temperature changes for 4 days (38.5°C for 12 hrs/35.5°C for 12 hrs, or vice versa), before returning to a constant 37°C. As a control, another IVD explant from the same mouse was incubated under constant 37°C. The PER2::Luc rhythms in IVD explants were all in similar circadian phase for the first 3 days before the temperature protocol (Fig. 1D). Once the antiphasic protocol was introduced, the oscillations were driven 180 ° out of phase with each other. Interestingly, the antiphasic oscillations were maintained for at least three more days after the tissues were released to constant temperature. In contrast, the IVD explant that remained at constant temperature gradually lost its ability to oscillate by day 7, mainly due to desynchronization in culture (Fig. 1D). These results clearly indicate that temperature cycles that approximate body temperature changes are capable of not only entraining the circadian phase of the IVD oscillation, but enhancing the oscillation amplitude.

Aging affects the circadian rhythm of IVDs

Daily systemic time cues in body temperature and hormone release are known to be altered with aging.[23] In addition, intrinsic properties of the clock oscillator could deteriorate with age as well.[23 24] Indeed, we have previously demonstrated that the amplitude of circadian oscillations in cartilage and tendon tissues dampen with aging.[25 26] Therefore, we hypothesized that circadian rhythms may change in aging disc, compromising the daily control of IVD physiology. To assess this, we compared the oscillations of PER2::Luc expression in mouse IVD explant cultures from animals aged 2 and 12 months (Fig. 2A, supplementary Video 1). The amplitude of oscillations in IVDs from 12 months old mice was severely reduced (by ~60%) as compared to 2 month old mice. Additionally, the average period of oscillations was significantly lengthened by 1.6 hrs in IVDs from 12 month old mice (Fig. 2A). IHC staining showed decreased expression of the core circadian transcription factors BMAL1 and CLOCK in 12 month (Fig. S1) and 24 month old mice as compared to 2

month old (Fig. 2B). These data demonstrate that the IVD clock becomes dysregulated with ageing.

The circadian rhythm of IVD is disrupted by IL-1β in a NF-κB dependent manner

Chronic inflammation is a known factor associated with IVD degeneration and lower back pain.[27] To investigate the effects of catabolic cytokines on disc circadian clock, we treated IVD explants from the PER2::Luc reporter mice with IL-1β, LPS and TNFα. Tissues were under continuous bioluminescence recording. Treatment with IL-1β (or LPS, Fig. S2A) resulted in complete disruption of the PER2::Luc circadian rhythm, associated with significant changes of clock genes (*Bmal1, Per2* and *Nr1d1*)(Fig. 3A, Fig.S3). The disrupted rhythm could be reinstated by dexamethasone (an anti-inflammatory glucocorticoid, Fig. 3A) or IL-1RA (an antagonist of IL-1, Fig.S2B), but not by forskolin (a clock synchronising agent without anti-inflammatory properties, Fig. S2C). NFκB is one of the classic pathways through which IL-1β can mediate its effects. To evaluate the involvement of NFκB, we used the IKK1/2 inhibitor BMS-345541 to block the activation of NFκB. The clock-disrupting effect of IL-1β was blocked by pre-treating the IVD explant with BMS-345541, supporting a role of NFκB pathway in the IL-1β -mediated clock disruption. In contrast to IL-1β, treatment of IVD explants with TNFα had no effect on their circadian rhythms (Fig. 3B). In contrast, both IL-1β and TNFα elicited a strong induction of NFκB signalling in a lung epithelial cell line, suggesting a possible cell-type specific response (Fig.S2D). Next, we took advantage of a transgenic mouse strain expressing the p65-DsRedXP protein fusion construct[28] to observe the nuclear translocation of p65, one of the major components of the NFκB complex. Live imaging showed that treatment of IVD explants with IL-1β caused rapid nuclear translocation of p65 both in AF and NP cells. However, addition of TNFα (up to 40 ng/mL) had no effect on p65 translocation (Fig.3C).

There are at least two potential mechanisms through which IL-1β could disrupt the IVD circadian rhythm. Individual cells may still have robust clocks but become desynchronised, with their clocks being in different phases, leading to reduced oscillation amplitude; or individual cells may have lost their pacemaking properties. To distinguish between these two possibilities, we used a high sensitivity EM-CCD camera to visualize the PER2::Luc bioluminescence signals from individual cells in the presence or absence of IL-1β. Consistent with the lack of effect of forskolin, this imaging approach revealed loss of bioluminescence at single cell level, excluding the desynchronization hypothesis (Fig. 3D and Supplementary video 2). Therefore, disruption to the IVD clock could be a hitherto undiscovered response to pro-inflammatory cytokines.

Identification of the first IVD circadian transcriptome

Circadian clocks in different tissues exert their local functions through regulating diverse yet highly tissue-specific set of target genes. To reveal the extent of rhythmic genes in IVD tissue under physiological conditions, we performed a time-series RNAseq study using IVD tissues (collected every 4 hours for 48 hours) from mice kept in 12 hr light/12 hr darkness. We used a well-recognized JTKCycle[29] algorithm to pick out rhythmic genes. Using P_{adjust}<0.05 as a cut-off, we identified 607 genes (3.5% of expressed genes in IVD) with rhythmic 24 hr expression patterns (Figure 4A, Supplementary Table 1). Further phase

clustering analysis of these rhythmic genes using R package revealed 4 main clusters (Fig. S4), with more than 70% of these genes peaking at night time points (representing the active phase of mouse). Gene ontology (GO)-term analysis using topGO revealed dozens of overrepresented functional groups with an adjusted $p< 0.01$, including "fatty acid metabolic process", "circadian rhythm", "intracellular protein transmembrane transport", "intrinsic apoptotic signaling pathway", "carboxylic acid metabolic process", and "response to endoplasmic reticulum stress". We next compared the IVD rhythmic gene list to that of the mouse cartilage and tendon we published earlier.[25 26] There was a very small number of genes (6-16%) overlapping between any two of these skeletal tissues, with only 16 genes common to all three, supporting the tissue-specific function of the peripheral clocks (Figure 4B). Of these 16 common genes, 8 were core circadian clock genes. The expression profiles of canonical clock genes (*Bmal1*, *Per2, Dbp*) and selected target genes *Follistatin* (a BMP antagonist)[30] *and Timp4* (a tissue inhibitor of MMPs)[31] relevant to IVD physiology and catabolism were validated by temporal qRT-PCR in mouse IVD tissues (Figure 4C, Fig S5).

Targeted deletion of *Bmal1* causes age-dependent IVD degeneration

Bmal1 is an essential circadian clock component for the generation of 24 hr rhythms. The global *Bmal1* knock-out mouse shows multi-tissue pathologies, including ectopic calcification of IVDs.[32] However, the severe disruption to whole body circadian rhythms confounds interpretation of phenotype. To evaluate the function of local IVD clocks, we produced a conditional KO mouse model (Col2a1-*Bmal1* KO, cKO) with a cell type-specific abolition of the transcription factor *Bmal1* in α1(II) collagen expressing cells, including NP and AF cells, and chondrocytes.[33] We have previously shown that the central SCN clock and behavioural locomotion rhythms in the cKO mice are not affected.[33] IHC staining of IVDs confirmed loss of BMAL1 expression in the majority of the AF cells and chondrocytes of the cartilaginous end plate in cKO mice (Fig. 5A). The cKO mouse was crossed with the PER2::Luc mouse to enable real-time tracking of clock rhythms. Photon counting of PER2::Luc bioluminescence demonstrated a lack of circadian oscillations in the cKO IVDs, with no response to dexamethasone treatment (Fig. 5B). Bioluminescence imaging of the cKO IVDs confirmed lack of circadian oscillations of PER2::Luc in both AF and NP cells (Fig. 5C and Supplementary video 3).

Histological analysis revealed early signs of degeneration of the lumbar IVDs in cKO mouse at 6 months of age, such as thinning of the growth plate of vertebral body (Fig. 6A), and gradual disappearance of the CEP (Fig. S6). At 12 months, there was widespread degeneration of lumbar IVDs in cKOs. Bone bridges appeared within the growth plate, the CEP was almost completely replaced by bone (Fig. 6A, black arrow), and the height of the disc was significantly reduced in cKO IVDs (Fig. 6A). In addition, staining with Safranin O and picrosirius red revealed disorganisation of the outer annulus structure and signs of fibrosis (with organized collagen bundles) appearing at the periphery of the IVDs (Fig. 6A-C, asterisk). Finally, using X-ray studies, the cKO mice showed clear signs of calcification and narrowing of spaces between vertebrae at 6 months (in tail IVDs, data not shown) and 12 months (in lumbar IVDs, Fig. 6C). No signs of degeneration were evident in age-matched WT mice up to the age of 12 months (Fig. 6B). However, similar degenerative changes to the cKO mutants were visible in WT mice at 24 months of age (Fig. S7), suggesting the possibility that loss of *Bmal1* and/or circadian rhythm in IVD cells leads to accelerated ageing of the tissue. TUNEL assay and qPCR were performed to explore the underlying

mechanisms for the observed phenotype. There were no obvious signs of apoptosis, although significant upregulation of catabolism-related genes (*Adamts1, Adamts5, Adamts15* and *Follistatin*) were observed in cKO IVDs (Fig.S8, S9). Together, these results indicate the essential role of the locally expressed core clock factor BMAL1 in IVD homeostasis, loss of which led to profound tissue degeneration.

Discussion

Low back pain is amongst the most prevalent spinal diseases associated with increasing age, with over 80% of the UK population predicted to experience back pain within their lifetime. Progressive degeneration of the IVD tissue, partly caused by increased catabolism driven by inflammatory/catabolic cytokines, is a major contributing factor in LBP.[34] It has long been known that the physiology of IVD is under strong influence by a diurnal rhythm associated with the rest/activity cycles, i.e., daily cycles of loading (activity phase) and low-load recovery (resting phase).[10-13] Exchange of nutrients/metabolites that occurs with fluid flow during this cycle maintains disc cell homeostasis. Recent epidemiological and experimental studies have linked shift work (in humans) and chronic disruption of circadian rhythms (in mice) to higher risk of IVD degeneration.[14 15 17-19] However, our study represents the first critical analysis of the molecular and cellular mechanisms of the IVD clock under physiological and pathological conditions. Using the clock gene reporter mouse/cell models, as well as a conditional *Bmal1* KO mouse model that had disrupted IVD clock, we established autonomous circadian clocks in mouse and human IVD cells that respond to temperature cycles, dampen with age and become dysregulated by catabolic cytokines. Genetic disruption to the mouse IVD molecular clock predisposes to IVD degeneration. Global *Bmal1* KO also showed a phenotype in the skeletal system, including the spine. However, our conditional KO model allows us to conclude the essential role of locally expressed BMAL1 or circadian rhythm in maintaining IVD homeostasis. These results support the notion that disruptions to circadian rhythms during ageing or in shift workers may be a contributing factor for the increased susceptibility to degenerative IVD diseases and low back pain.

We also revealed for the first time the circadian transcriptome of the IVD tissue. Of particular interest are the genes and pathways that have been previously implicated in IVD physiology and pathology, such as genes involved in matrix homeostasis/repair (e.g Follistatin, Timp4, Adamts1, Adamts5, Adamts15 and Adam17),[30 31] mitochondria function and fatty acid metabolism (e.g. Pex1, Pex2, Pex5, Pex15, Adipoq, Adipor2, Fasn).[35 36] Although glucose and anaerobic glycolysis represent major metabolic pathways in IVD, there is evidence that mitochondria in the NP are functional and they retain the capacity to metabolise fatty acids through mitochondrial oxidative metabolism.[35] Other relevant pathways include ER stress and apoptosis (e.g. Aifm1, Atf6, Chac1, Bak1, Bbc3, Opa1 and Fas).[37 38] The diverse clock-controlled pathways identified by this approach implicate circadian rhythm as a critical regulatory mechanism for IVD biology.

Using IVD tissue explants, we have identified the disruption of the circadian clock in IVD as hitherto undiscovered response to pro-inflammatory cytokines. Similar clock disruptions by inflammatory cytokines have been found in other cell types, such as in macrophages,[39]

synovial fibroblasts,[40] and chondrocytes.[28] The involvement of NFκB pathway in mediating the effects of IL-1 is consistent with our earlier findings in chondrocytes, where NFκB interferes with the core clock complex to disrupt circadian pacemaking.[28] Given the diverse pathways controlled by the IVD clock, cytokine-mediated circadian disruption may be involved in driving key aspects of the catabolic response of IVD to chronic inflammation. Therefore, there is the possibility of stabilizing IVD clock rhythm as a novel strategy to combat tissue catabolism. Although the concentration we used for IL-1β (5 ng/mL) in these tissue explant studies was higher than that in degenerative IVD (~50 pg/mL), this dose is in line with most *ex vivo*/*in vitro* studies. We also identified a lack of response of the IVD clock (and cartilage clock)[28] to TNFα, possibly due to the defective NFκB nuclear translocation. These findings suggest IL-1 and TNFα may act on distinct downstream pathways and regulate different target genes within the IVD, as seen in chondrocytes. In SW1353 chondrocyte-derived cells, catabolic genes such as IL-6, BMP-2, MMP13 and COX-2 only respond to IL-1, with almost no response to TNFα.[41 42] Such results are intriguing because we have shown that IL-1β plays a more prominent role in driving disc degeneration than TNFα.[43 44] Therefore, anti-inflammatory drugs that selectively target IL-1 are more likely to bring therapeutic benefits.

In conclusion, our results provide a firm basis for future studies that aim to elucidate the functional implication and therapeutic potential of the human IVD circadian rhythm in health and disease of the spine.

References

1 Hastings MH, Reddy AB, Maywood ES. A clockwork web: circadian timing in brain and periphery, in health and disease. *Nat Rev Neurosci* 2003;4(8):649-61.

2 Partch CL, Green CB, Takahashi JS. Molecular architecture of the mammalian circadian clock. *Trends Cell Biol* 2014;24(2):90-9.

3 Reppert SM, Weaver DR. Coordination of circadian timing in mammals. *Nature* 2002;418(6901):935-41.

4 Bass J, Takahashi JS. Circadian integration of metabolism and energetics. *Science* 2010;330(6009):1349-54.

5 Dudek M, Meng QJ. Running on time: the role of circadian clocks in the musculoskeletal system. *Biochem J* 2014;463(1):1-8.

6 Takahashi JS, Hong HK, Ko CH, *et al*. The genetics of mammalian circadian order and disorder: implications for physiology and disease. *Nat Rev Genet* 2008;9(10):764-75.

7 Zhang R, Lahens NF, Ballance HI, *et al*. A circadian gene expression atlas in mammals: implications for biology and medicine. *Proc Natl Acad Sci USA* 2014;111(45):16219-24.

8 Boden SD, Davis DO, Dina TS, *et al*. Abnormal magnetic-resonance scans of the lumbar spine in asymptomatic subjects. A prospective investigation. *J Bone Joint Surg Am* 1990;72(3):403-8.

9 Global Burden of Disease Study C. Global, regional, and national incidence, prevalence, and years lived with disability for 301 acute and chronic diseases and injuries in 188 countries, 1990-2013: a systematic analysis for the Global Burden of Disease Study 2013. *Lancet* 2015;386(9995):743-800.

10 Haschtmann D, Stoyanov JV, Ferguson SJ. Influence of diurnal hyperosmotic loading on the metabolism and matrix gene expression of a whole-organ intervertebral disc model. *J Orthop Res* 2006;24(10):1957-66.

11 Malko JA, Hutton WC, Fajman WA. An in vivo magnetic resonance imaging study of changes in the volume (and fluid content) of the lumbar intervertebral discs during a simulated diurnal load cycle. *Spine* 1999;24(10):1015-22.

12 Matsumoto T, Kawakami M, Kuribayashi K, *et al*. Cyclic mechanical stretch stress increases the growth rate and collagen synthesis of nucleus pulposus cells in vitro. *Spine* 1999;24(4):315-9.

13 van der Veen AJ, van Dieen JH, Nadort A, *et al*. Intervertebral disc recovery after dynamic or static loading in vitro: is there a role for the endplate? *J Biomech* 2007;40(10):2230-5.

14 Elfering A, Semmer N, Birkhofer D, *et al*. Risk factors for lumbar disc degeneration: a 5-year prospective MRI study in asymptomatic individuals. *Spine* 2002;27(2):125-34.

15 Kaila-Kangas L, Kivimaki M, Harma M, *et al*. Sleep disturbances as predictors of hospitalization for back disorders-a 28-year follow-up of industrial employees. *Spine* 2006;31(1):51-6.

16 Leino-Arjas P, Kaila-Kangas L, Kauppinen T, *et al*. Occupational exposures and inpatient hospital care for lumbar intervertebral disc disorders among Finns. *Am J Ind Med* 2004;46(5):513-20.

17 Rajaratnam SM, Arendt J. Health in a 24-h society. *Lancet* 2001;358(9286):999-1005.

18 Zhao I, Bogossian F, Turner C. The effects of shift work and interaction between shift work and overweight/obesity on low back pain in nurses: results from a longitudinal study. *J Occup Environ Med* 2012;54(7):820-5.

19 Kc R, Li X, Forsyth CB, Voigt RM, *et al*. Osteoarthritis-like pathologic changes in the knee joint induced by environmental disruption of circadian rhythms is potentiated by a high-fat diet. *Sci Rep* 2015;5:16896.

20 Numaguchi S, Esumi M, Sakamoto M, *et al*. Passive cigarette smoking changes the circadian rhythm of clock genes in rat intervertebral discs. *J Orthop Res* 2016;34(1):39-47.

21 Yoo SH, Yamazaki S, Lowrey PL, *et al*. PERIOD2::LUCIFERASE real-time reporting of circadian dynamics reveals persistent circadian oscillations in mouse peripheral tissues. *Proc Natl Acad Sci USA* 2004;101(15):5339-46.

22 Freemont AJ, Peacock TE, Goupille P, *et al*. Nerve ingrowth into diseased intervertebral disc in chronic back pain. *Lancet* 1997;350(9072):178-81.

23 Brown SA, Pagani L, Cajochen C, *et al*. Systemic and cellular reflections on ageing and the circadian oscillator: a mini-review. *Gerontology* 2011;57(5):427-34.

24 Davidson AJ, Yamazaki S, Arble DM, *et al*. Resetting of central and peripheral circadian oscillators in aged rats. *Neurobiol Aging* 2008;29(3):471-7.

25 Gossan N, Zeef L, Hensman J, *et al*. The circadian clock in murine chondrocytes regulates genes controlling key aspects of cartilage homeostasis. *Arthritis Rheum* 2013;65(9):2334-45.

26 Yeung CY, Gossan N, Lu Y, *et al*. Gremlin-2 is a BMP antagonist that is regulated by the circadian clock. *Sci Rep* 2014;4:5183.

27 Molinos M, Almeida CR, Caldeira J, *et al*. Inflammation in intervertebral disc degeneration and regeneration. *J R Soc Interface* 2015;12(108):20150429.

28 Guo B, Yang N, Borysiewicz E, *et al*. Catabolic cytokines disrupt the circadian clock and the expression of clock-controlled genes in cartilage via an NFsmall ka, CyrillicB-dependent pathway. *Osteoarthritis Cartilage* 2015;23(11):1981-8.

29 Hughes ME, Hogenesch JB, Kornacker K. JTK_CYCLE: an efficient nonparametric algorithm for detecting rhythmic components in genome-scale data sets. *J Biol Rhythms* 2010;25(5):372-80.

30 McMahon JA, Takada S, Zimmerman LB, *et al*. Noggin-mediated antagonism of BMP signaling is required for growth and patterning of the neural tube and somite. *Genes Dev* 1998;12(10):1438-52.

31 Vo NV, Hartman RA, Yurube T, *et al*. Expression and regulation of metalloproteinases and their inhibitors in intervertebral disc aging and degeneration. *Spine J* 2013;13(3):331-41.
32 Bunger MK, Walisser JA, Sullivan R, *et al*. Progressive arthropathy in mice with a targeted disruption of the Mop3/Bmal-1 locus. *Genesis* 2005;41(3):122-32.
33 Dudek M, Gossan N, Yang N *et al*. The chondrocyte clock gene Bmal1 controls cartilage homeostasis and integrity. *J Clin Invest* 2016;126(1):365-76.
34 Luoma K, Riihimaki H, Luukkonen R, *et al*. Low back pain in relation to lumbar disc degeneration. *Spine* 2000;25(4):487-92.
35 Agrawal A, Guttapalli A, Narayan S, *et al*. Normoxic stabilization of HIF-1alpha drives glycolytic metabolism and regulates aggrecan gene expression in nucleus pulposus cells of the rat intervertebral disk. *Am J Physiol Cell Physiol* 2007;293(2):C621-31.
36 Rannou F, Lee TS, Zhou RH, *et al*. Intervertebral disc degeneration: the role of the mitochondrial pathway in annulus fibrosus cell apoptosis induced by overload. *Am J Pathol* 2004;164(3):915-24.
37 Lee HW, Kim SY, Kim AY, *et al*. Adiponectin stimulates osteoblast differentiation through induction of COX2 in mesenchymal progenitor cells. *Stem cells* 2009;27(9):2254-62.
38 Wang H, Liu H, Zheng ZM, *et al*. Role of death receptor, mitochondrial and endoplasmic reticulum pathways in different stages of degenerative human lumbar disc. *Apoptosis* 2011;16(10):990-1003.
39 Spengler ML, Kuropatwinski KK, Comas M, *et al*. Core circadian protein CLOCK is a positive regulator of NF-kappaB-mediated transcription. *Proc Natl Acad Sci USA* 2012;109(37):E2457-65.
40 Haas S, Straub RH. Disruption of rhythms of molecular clocks in primary synovial fibroblasts of patients with osteoarthritis and rheumatoid arthritis, role of IL-1beta/TNF. *Arthritis Res Ther* 2012;14(3):R122.
41 Shi J, Schmitt-Talbot E, DiMattia DA, *et al*. The differential effects of IL-1 and TNF-alpha on proinflammatory cytokine and matrix metalloproteinase expression in human chondrosarcoma cells. *Inflamm Res* 2004;53(8):377-89.
42 Tetlow LC, Adlam DJ, Woolley DE. Matrix metalloproteinase and proinflammatory cytokine production by chondrocytes of human osteoarthritic cartilage: associations with degenerative changes. *Arthritis Rheum* 2001;44(3):585-94.
43 Hoyland JA, Le Maitre C, Freemont AJ. Investigation of the role of IL-1 and TNF in matrix degradation in the intervertebral disc. *Rheumatology* 2008;47(6):809-14.
44 Le Maitre CL, Hoyland JA, Freemont AJ. Catabolic cytokine expression in degenerate and herniated human intervertebral discs: IL-1beta and TNFalpha expression profile. *Arthritis Res Ther* 2007;9(4):R77.
45 Storch KF, Paz C, Signorovitch J, *et al*. Intrinsic circadian clock of the mammalian retina: importance for retinal processing of visual information. *Cell* 2007;130(4):730-41.
46 Sakai K, Hiripi L, Glumoff V, *et al*. Stage-and tissue-specific expression of a Col2a1-Cre fusion gene in transgenic mice. *Matrix Biol* 2001;19(8):761-7.
47 Sladek M, Rybova M, Jindrakova Z, *et al*. Insight into the circadian clock within rat colonic epithelial cells. *Gastroenterology* 2007;133(4):1240-9.
48 J AAaR. topGO: topGO: Enrichment analysis for Gene Ontology. R package version 2.22.0. 2010.
49 J K. Rtsne: T-Distributed Stochastic Neighbor Embedding using Barnes-Hut Implementation, 2015.
50 Sive JI, Baird P, Jeziorsk M, *et al*. Expression of chondrocyte markers by cells of normal and degenerate intervertebral discs. *Mol Pathol* 2002;55(2):91-7.

Figure legends

Figure 1. IVDs possess an autonomous circadian clock. (A) Representative PER2::Luc bioluminescence trace of mouse IVD explant culture (period = 23.93 ± 0.247h; mean ± SD; n=6); (B) Representative trace of human NP cells transduced with a *Per2::luc* reporter (period=22.52 ± 0.39h; mean ± SD; n=3); (C) IHC of BMAL1 and CLOCK on NP biopsy of human IVDs (magnification 5x left, 10x right); n=3. (D) Temperature entrainment (n=4). Two IVD explant cultures (represented by red and blue traces) from the same animal were held under antiphase temperature cycles (alternating 12-hour cycles of 38.5°C/35.5°C; baseline temperature= 37°C). Third IVD explant culture from the same animal was kept at a constant temperature of 37°C (Purple trace below).

Figure 2. Circadian rhythm of IVD is dampened during aging. (A) Representative bioluminescence traces of young (2 months) and ageing (12 months) IVDs from PER2::Luc mice. The period was significantly lengthened in older mice ($p<0.05$) and the amplitude was significantly dampened ($p<0.05$) (two-tailed nonparametric Mann-Whitney test; n=4); (B) IHC of BMAL1 and CLOCK on young (3 months) and aged (24 months) mouse IVDs; n=4. Magnification 10x. The Safranin O staining panel on the right was included to ease visualization of the different structures of the IVD. NP- nucleus pulposus; AF- annulus fibrosus; OAF- outer annulus fibrosus; CEP- cartilaginous end plate.

Figure 3. IL-1β, but not TNFα, disrupts the circadian rhythm of IVDs. (A) Representative bioluminescence traces of PER2::Luc mouse IVD explants. Arrows indicate time of treatment with IL-1β (5 ng/mL), IKK inhibitor (BMS-345541, 10 μM) and dexamethasone (100 nM). Red trace - treated with IL-1β, green trace - pre-treated with IKK inhibitor before addition of IL-1β, blue trace - vehicle control; n=3. (B) Representative bioluminescence traces treated with TNFα (red trace, 40 ng/mL) or control (blue trace). Arrows indicate time of treatments; n=3. (C) Live fluorescence imaging of p65DsRed reporter in mouse IVDs by confocal microscopy before and after treatment with IL-1β or TNFα. Scale bar 20 μm. Arrows indicate the nuclei. AF- annulus fibrosus; NP- nucleus pulposus; (D) Live bioluminescence imaging of an IVD tissue from PER2::Luc mouse, treated with IL-1β (at 48h), followed by dexamethasone (at 96h).

Figure 4. Circadian transcriptome in mouse IVD identified by time series RNA sequencing. (A) Heat map depicting the expression patterns of the 607 rhythmic genes (3.5 % of the IVD transcriptome) identified by JTKCycle. Genes were organized according to timing of peak expression. White bars represent the day; black bars represent the night. (B) Venn diagram comparing the number of rhythmic genes of IVD, cartilage and tendon. (C) qPCR validation of time-dependent expression of clock genes (*Bmal1, Per2* and *Dbp)* and target genes (*Follistatin* and *Timp4*) in mouse IVDs normalized to *Gapdh*. Mean and SEM (n = 6). Grey shadow indicates the night phase.

Figure 5. Conditional deletion of *Bmal1* in *Col2a1*-expressing cells results in disruption of the circadian rhythms in mouse IVDs. (A) IHC of BMAL1 in 3 month old WT and KO mice (magnification: upper panels 10x and lower panels 40x); n=3. (B) Representative bioluminescence traces of WT (blue) and *Bmal1* cKO (red) mouse IVD explant cultures; n=6. Arrow indicates treatment with dexamethasone. (C) Live bioluminescence imaging of IVDs from WT and *Bmal1* cKO IVDs from mice on a PER2::Luc background.

Figure 6. Loss of *Bmal1* leads to degeneration of IVDs and cartilaginous tissues of the spine. (A) Safranin O staining of 12 month old WT and *Bmal1* cKO mouse lumbar IVDs; n=4. Red arrow-loss of CEP; Black arrow- fragmentation of growth plate; *-fibrosis (magnification 2.5x). Analysis of the IVD height and growth plate thickness was shown (two-tailed nonparametric Mann-Whitney test; n=4) *- p<0.05; *** - p<0.001. (B) Picrosirius red staining of lumbar IVDs from 12 month old WT and *Bmal1* cKO mouse showing organisation of collagen (magnification 2.5x left and 5x right panels); n=4. Images were visualized under brightfield or polarized light. (C) X-ray radiography of 12 month old WT and *Bmal1* cKO mouse spines; n=3. Yellow arrows- calcification of IVDs; Red arrows- calcification of tissues surrounding the IVDs.

Supplementary figure legends

Figure S1. Reduced expression of BMAL1 and CLOCK in ageing IVDs. IHC of BMAL1 and CLOCK on sections of IVDs from 3 and 12 months old mice; n=4. Magnification, 5x left and middle panels, 10x right panels. BMAL1 staining was visible in the AF, but not the CEP, of 12 month old mice. CLOCK staining was largely absent in both AF and CEP in 12 month old mice.

Figure S2. Effects of LPS, IL-1RA, forskolin and TNFα on IVD oscillations. Representative bioluminescence traces of PER2::Luc mouse IVD explants; n=3. (A) LPS treatment (1 μg/mL, red trace) disrupted the rhythm, which could be rescued by treatment with dexamethasone (100 nM). (B, C) Disrupted circadian rhythm by IL-1β treatment (5 ng/mL, red trace) was not rescued by application of forskolin (10 μM), but by pre-treatment with IL-1RA (1 μg/mL) . Arrows indicate time of treatment. (D) Both IL-1β (5 ng/mL) and TNFα (40 ng/mL) induced strong NFkB signalling in lung epithelial cells stably transfected with NFκB::luc reporter. Representative, n=3.

Figure S3. Effects of IL-1β on endogenous clock gene expression. qPCR of several clock genes, *Adamts1* and *IL-6* in IVD explants upon IL-1β treatment (5 ng/mL for 4 hours). *, p<0.05; ***, p<0.001, n=4.

Figure S4. Phase clustering analysis of rhythmic genes in mouse IVDs. Clustering analysis was performed using cluster (A) and Rtsne (B) of R package. These analyses revealed 4 main clusters with different peak times (two at night and two during the day). Example genes for each cluster were highlighted. There was a good concordance between these two methods of analysis.

Figure S5. Time course qPCR of *β-actin* in mouse IVDs. Note the lack of circadian rhythms. Mean and SEM (n = 6).

Figure S6. Early onset of IVD degeneration in IVDs from 6 month old cKO mice. Safranin O/methyl green staining revealed gradual disappearance of CEP in the *Bmal1* cKO mouse (black arrow); n=4.

Figure S7. Spontaneous degeneration of IVDs from aged WT mice. Picrosirius red staining and polarised light microscopy were performed on IVDs from 3 and 24 month old wild type mice; n=4. The aged WT mouse IVDs display a phenotype similar to *Bmal1* cKO IVDs, with fibrosis of the outer AF composed of bundles of organised collagen visible under polarised light microscope.

Figure S8. TUNEL staining of IVDs from 12 months old WT and *Bmal1* cKO mice. Note there were no detectable signs of apoptosis in either WT or cKO IVDs. N=4.

Figure S9. Time course qPCR of catabolic genes in IVDs from 3 months old WT and *Bmal1* cKO mice. Mean and SEM (n = 4). *, p<0.05; **, p<0.01; ***, p<0.001.

Supplementary table and videos

Supplementary Table 1. List of rhythmic IVD genes with a ~24 hr period.

Supplementary Video 1, Live bioluminescence imaging of the PER2::Luc mouse IVD explants (2 month on the left and 12 month on the right) using high sensitivity EM-CCD camera.

Supplementary Video 2, Live bioluminescence imaging of the PER2::Luc mouse IVD explants treated with IL-1β (at 48 hr), followed by Dex (at 96 hr).

Supplementary Video 3, Live bioluminescence imaging of the mouse IVD explants from a WT mouse (left) and a *Bmal1* cKO mouse (right).

Funding
This work was funded by a Medical Research Council (MRC) UK Career Development Award (G0900414, to Q.J. Meng); an Arthritis Research UK Senior Research Fellowship Award (20875, to Q.J. Meng); an MRC project grant (MR/K019392/1, to Q.J. Meng and R.P. Boot-Handford); a Wellcome Trust (UK) Core funding grant (088785/Z/09/Z) to the University of Manchester Wellcome Trust Centre for Cell Matrix Research. Consumables for processing of human IVD and isolation and culture of human IVD cells were funded by the National Institute for Health Research Manchester Musculoskeletal Biomedical Research Unit. The Funders had no role in the study design, data interpretation, report and submission of this work.

Fig 1

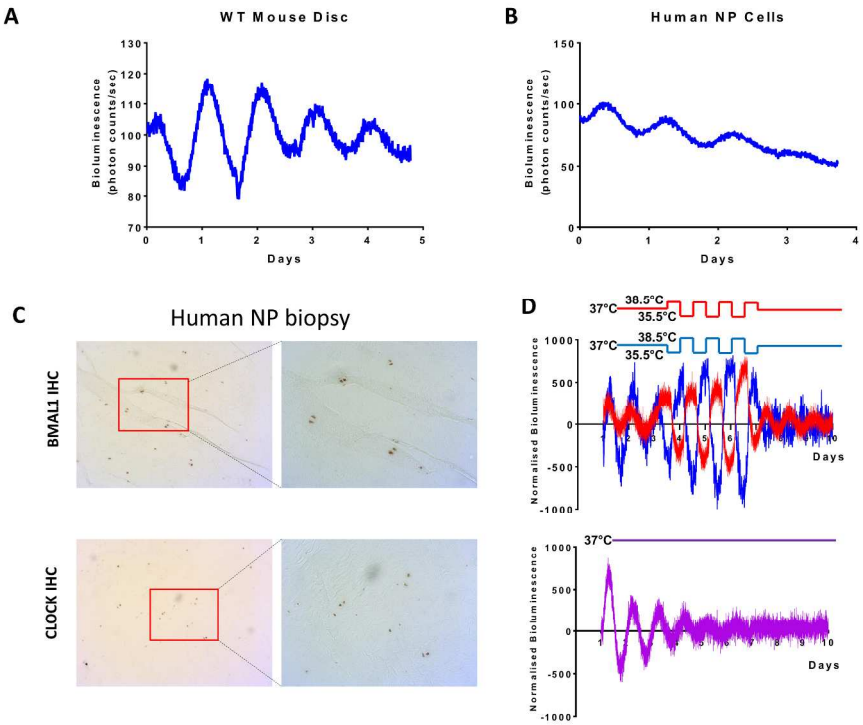

Figure 1. IVDs possess an autonomous circadian clock. (A) Representative PER2::Luc bioluminescence trace of mouse IVD explant culture (period = 23.93 ± 0.247h; mean ± SD; n=6); (B) Representative trace of human NP cells transduced with a Per2::luc reporter (period=22.52 ± 0.39h; mean ± SD; n=3); (C) IHC of BMAL1 and CLOCK on NP biopsy of human IVDs (magnification 5x left, 10x right); n=3. (D) Temperature entrainment (n=4). Two IVD explant cultures (represented by red and blue traces) from the same animal were held under antiphase temperature cycles (alternating 12-hour cycles of 38.5°C/35.5°C; baseline temperature= 37°C). Third IVD explant culture from the same animal was kept at a constant temperature of 37°C (Purple trace below).

254x190mm (300 x 300 DPI)

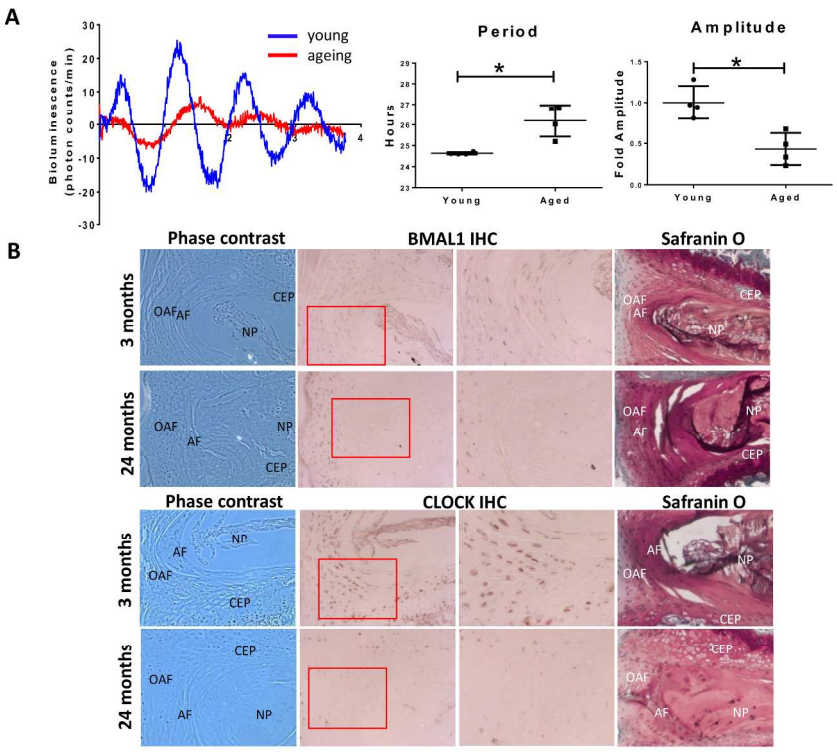

Fig 2

Figure 2. Circadian rhythm of IVD is dampened during aging. (A) Representative bioluminescence traces of young (2 months) and ageing (12 months) IVDs from PER2::Luc mice. The period was significantly lengthened in older mice ($p<0.05$) and the amplitude was significantly dampened ($p<0.05$) (two-tailed nonparametric Mann-Whitney test; n=4); (B) IHC of BMAL1 and CLOCK on young (3 months) and aged (24 months) mouse IVDs; n=4. Magnification 10x. The Safranin O staining panel on the right was included to ease visualization of the different structures of the IVD. NP- nucleus pulposus; AF- annulus fibrosus; OAF- outer annulus fibrosus; CEP- cartilaginous end plate.

254x190mm (300 x 300 DPI)

Fig 3

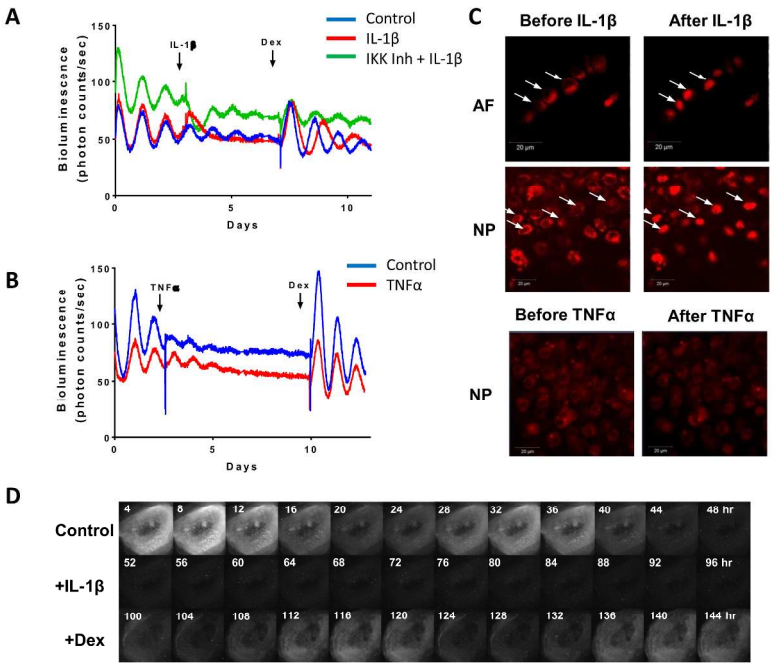

Figure 3. IL-1β, but not TNFα, disrupts the circadian rhythm of IVDs. (A) Representative bioluminescence traces of PER2::Luc mouse IVD explants. Arrows indicate time of treatment with IL-1β (5 ng/mL), IKK inhibitor (BMS-345541, 10 μM) and dexamethasone (100 nM). Red trace - treated with IL-1β, green trace - pre-treated with IKK inhibitor before addition of IL-1β, blue trace - vehicle control; n=3. (B) Representative bioluminescence traces treated with TNFα (red trace, 40 ng/mL) or control (blue trace). Arrows indicate time of treatments; n=3. (C) Live fluorescence imaging of p65DsRed reporter in mouse IVDs by confocal microscopy before and after treatment with IL-1β or TNFα. Scale bar 20 μm. Arrows indicate the nuclei. AF- annulus fibrosus; NP- nucleus pulposus; (D) Live bioluminescence imaging of an IVD tissue from PER2::Luc mouse, treated with IL-1β (at 48h), followed by dexamethasone (at 96h).

254x190mm (300 x 300 DPI)

Fig 4

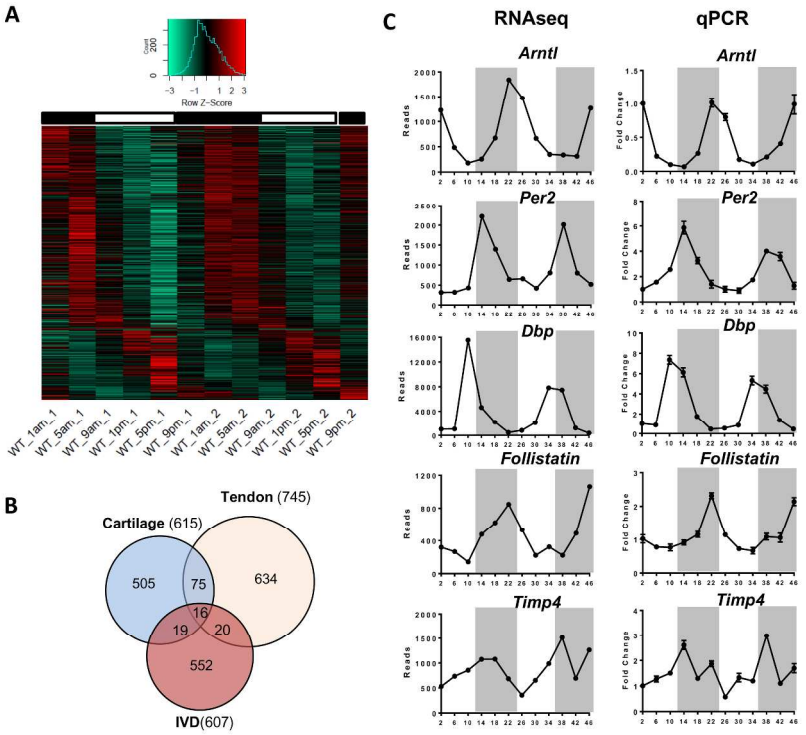

Figure 4. Circadian transcriptome in mouse IVD identified by time series RNA sequencing. (A) Heat map depicting the expression patterns of the 607 rhythmic genes (3.5 % of the IVD transcriptome) identified by JTKCycle. Genes were organized according to timing of peak expression. White bars represent the day; black bars represent the night. (B) Venn diagram comparing the number of rhythmic genes of IVD, cartilage and tendon. (C) qPCR validation of time-dependent expression of clock genes (Bmal1, Per2 and Dbp) and target genes (Follistatin and Timp4) in mouse IVDs normalized to Gapdh. Mean and SEM (n = 6). Grey shadow indicates the night phase.

254x190mm (300 x 300 DPI)

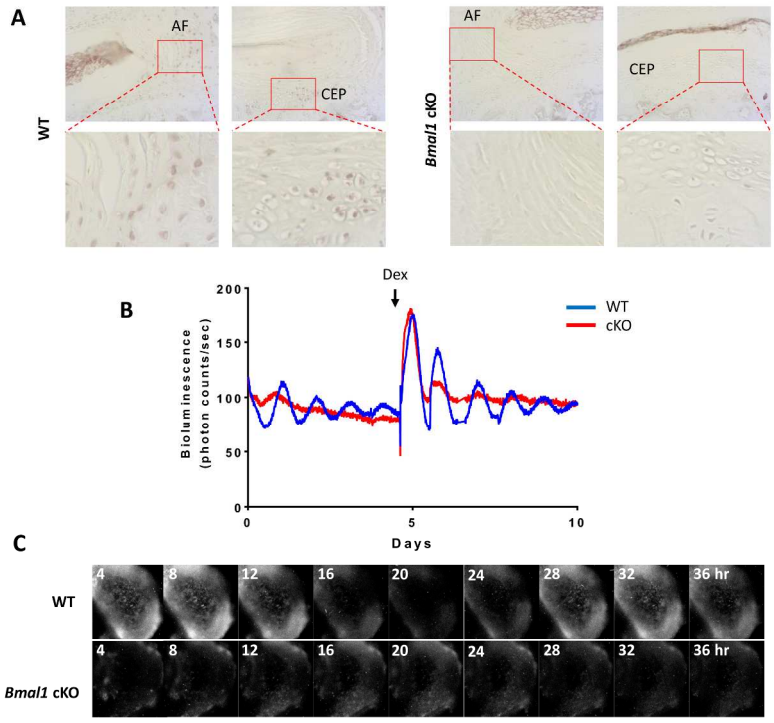

Fig 5

Figure 5. Conditional deletion of Bmal1 in Col2a1-expressing cells results in disruption of the circadian rhythms in mouse IVDs. (A) IHC of BMAL1 in 3 month old WT and KO mice (magnification: upper panels 10x and lower panels 40x); n=3. (B) Representative bioluminescence traces of WT (blue) and Bmal1 cKO (red) mouse IVD explant cultures; n=6. Arrow indicates treatment with dexamethasone. (C) Live bioluminescence imaging of IVDs from WT and Bmal1 cKO IVDs from mice on a PER2::Luc background.

254x190mm (300 x 300 DPI)

Fig 6

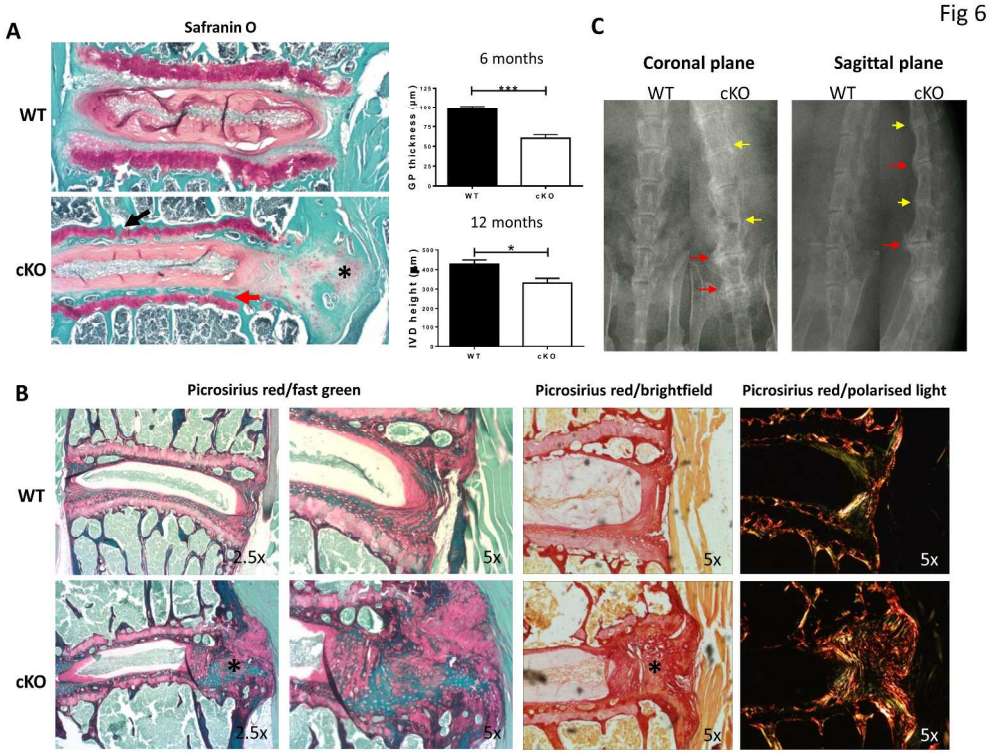

Figure 6. Loss of Bmal1 leads to degeneration of IVDs and cartilaginous tissues of the spine. (A) Safranin O staining of 12 month old WT and Bmal1 cKO mouse lumbar IVDs; n=4. Red arrow-loss of CEP; Black arrow-fragmentation of growth plate; *-fibrosis (magnification 2.5x). Analysis of the IVD height and growth plate thickness was shown (two-tailed nonparametric Mann-Whitney test; n=4) *- $p<0.05$; *** - $p<0.001$. (B) Picrosirius red staining of lumbar IVDs from 12 month old WT and Bmal1 cKO mouse showing organisation of collagen (magnification 2.5x left and 5x right panels); n=4. Images were visualized under brightfield or polarized light. (C) X-ray radiography of 12 month old WT and Bmal1 cKO mouse spines; n=3. Yellow arrows- calcification of IVDs; Red arrows- calcification of tissues surrounding the IVDs.

254x190mm (300 x 300 DPI)

Fig S1

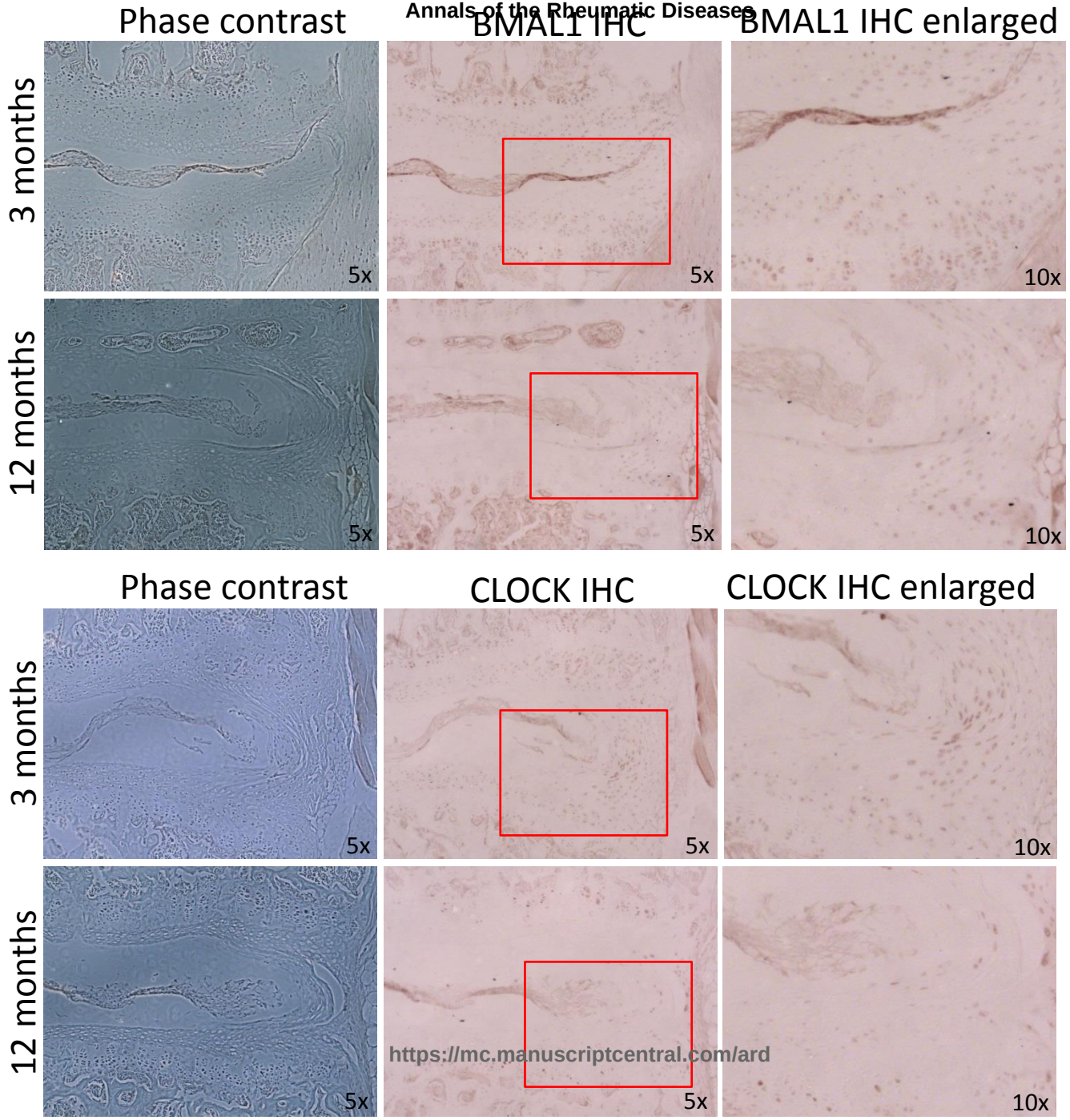

Fig S2

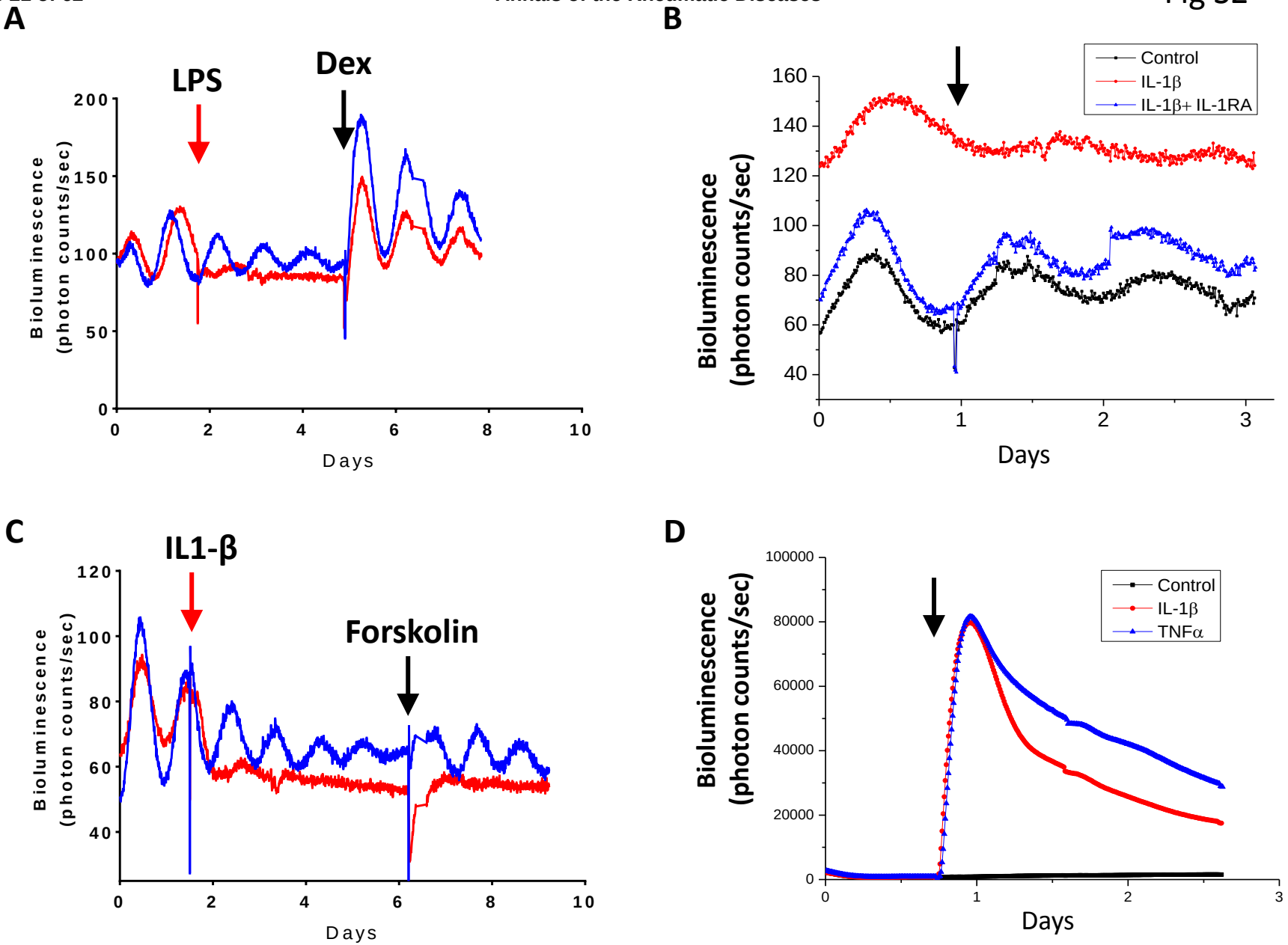
A
LPS
Dex
Bioluminescence (photon counts/sec)
Days
B
Control
IL-1β
IL-1β+ IL-1RA
Bioluminescence (photon counts/sec)
Days
C
IL1-β
Forskolin
Bioluminescence (photon counts/sec)
Days
D
Control
IL-1β
TNFα
Bioluminescence (photon counts/sec)
Days

Fig S3

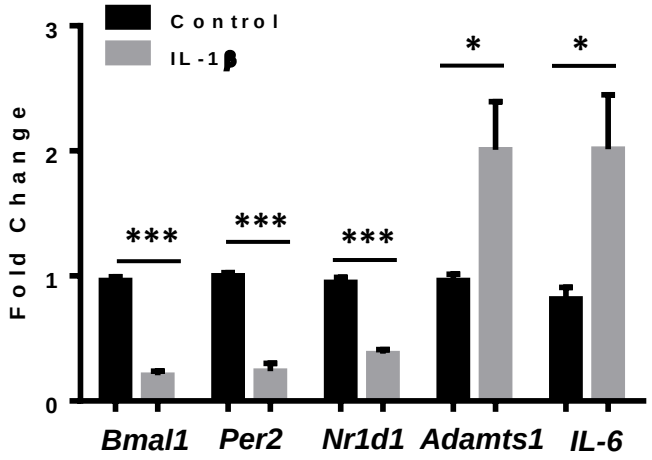

Fig S4

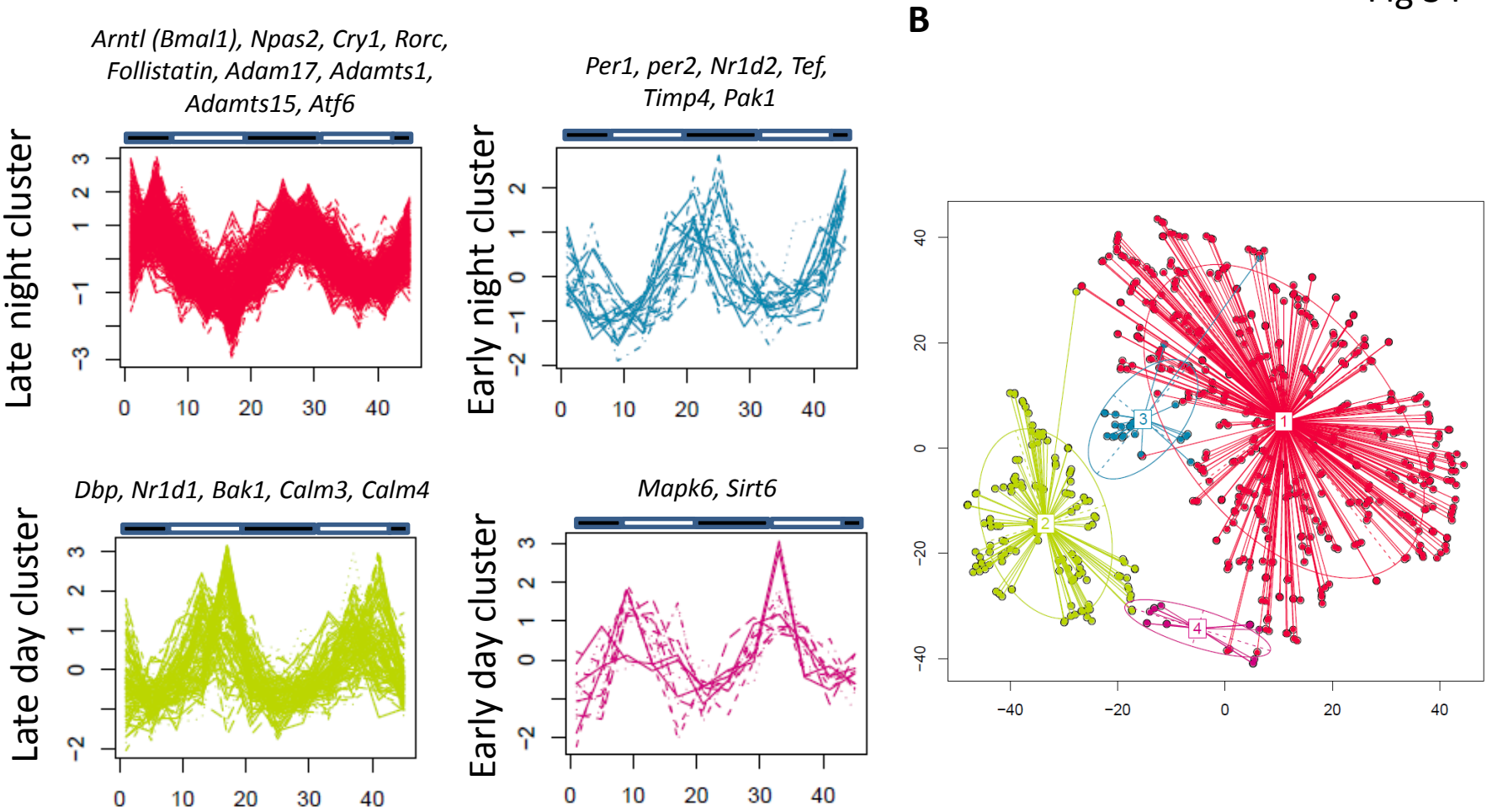
A
Arntl (Bmal1), Npas2, Cry1, Rorc, Follistatin, Adam17, Adamts1, Adamts15, Atf6
Per1, per2, Nr1d2, Tef, Timp4, Pak1
Dbp, Nr1d1, Bak1, Calm3, Calm4
Mapk6, Sirt6
Late night cluster
Early night cluster
Late day cluster
Early day cluster
B
1
2
3
4

Fig S5

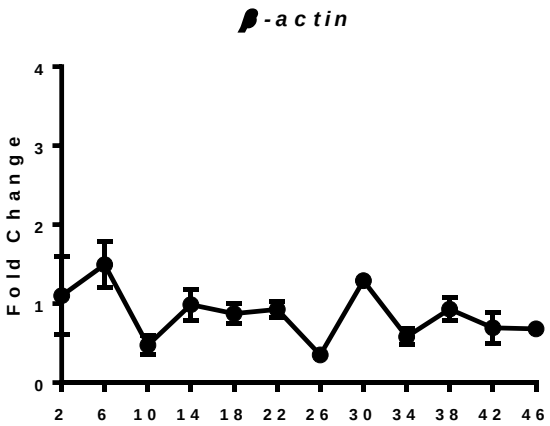
β-actin
Fold Change
0
1
2
3
4
2 6 10 14 18 22 26 30 34 38 42 46
Circadian time, hrs

Fig S6

6months

WT

cKO

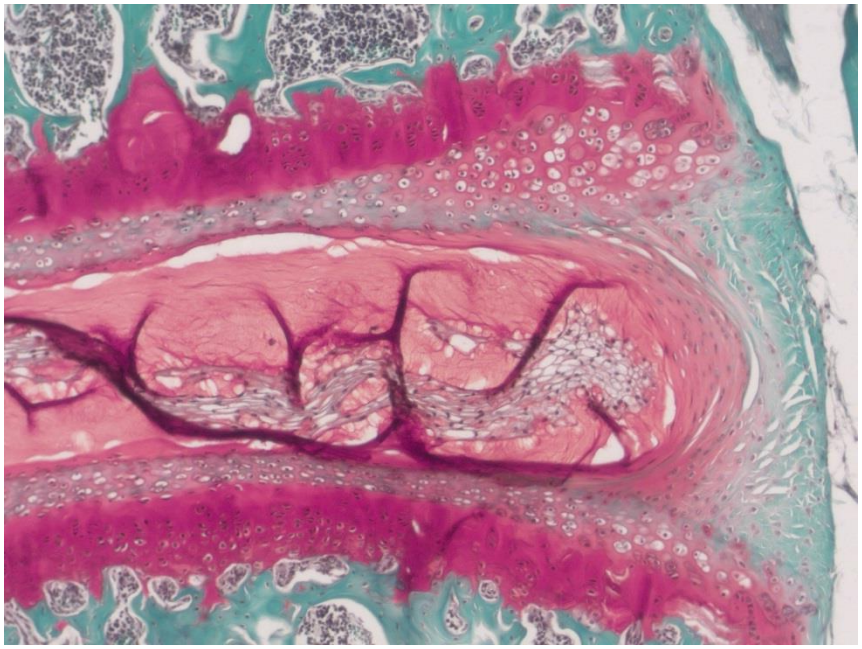

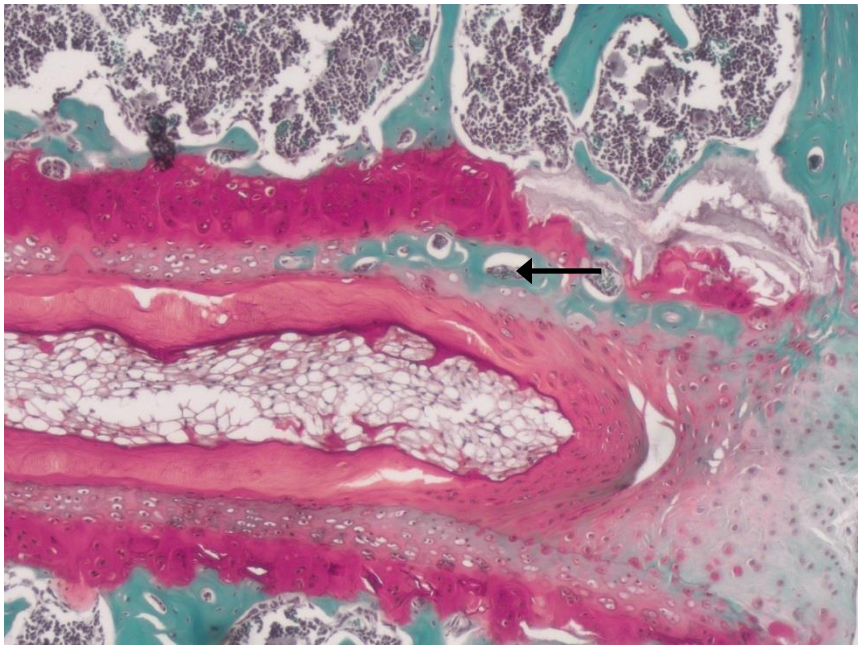

Fig S7

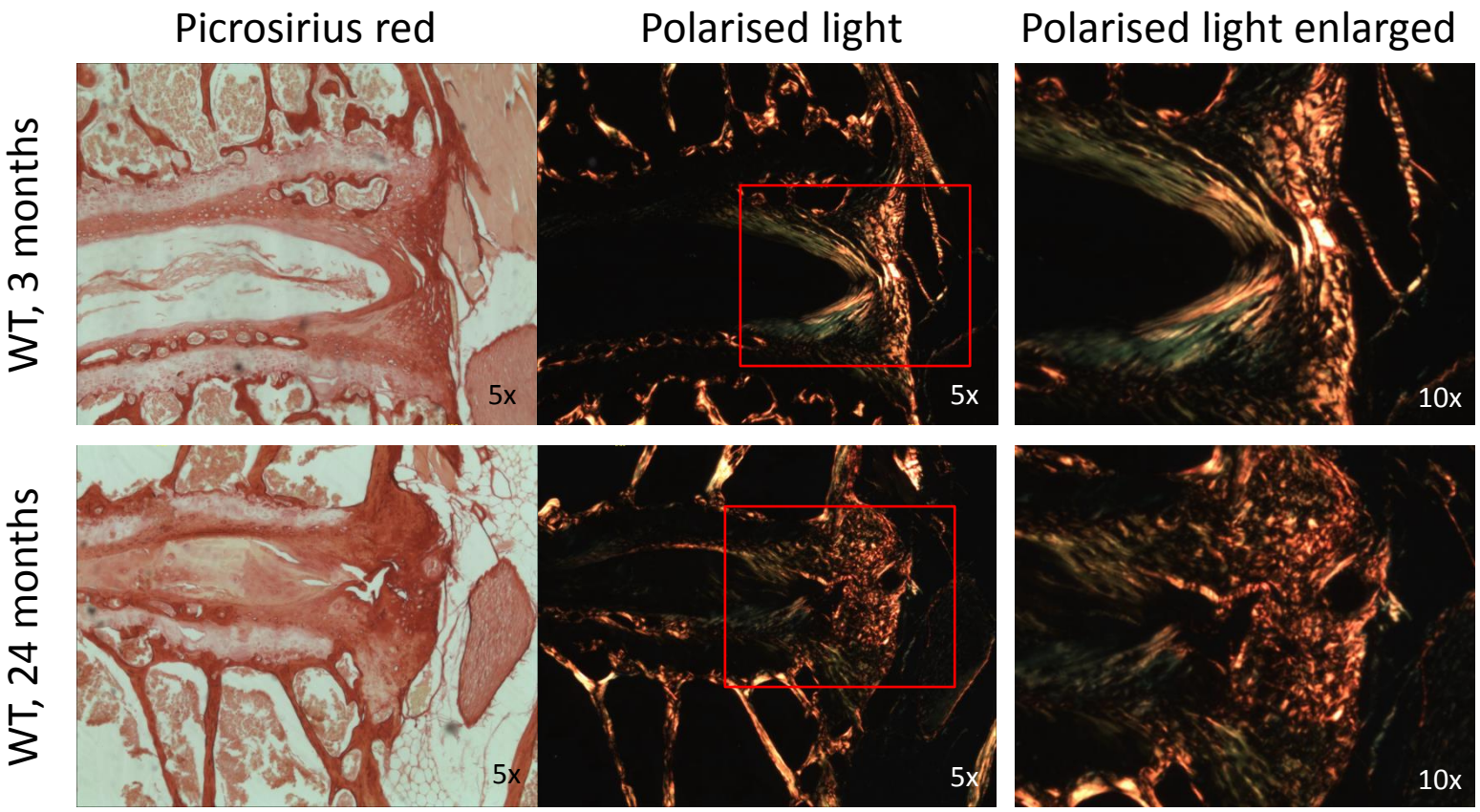
Picrosirius red
Polarised light
Polarised light enlarged
WT, 3 months
WT, 24 months
5x
5x
10x
5x
5x
10x

Fig S8

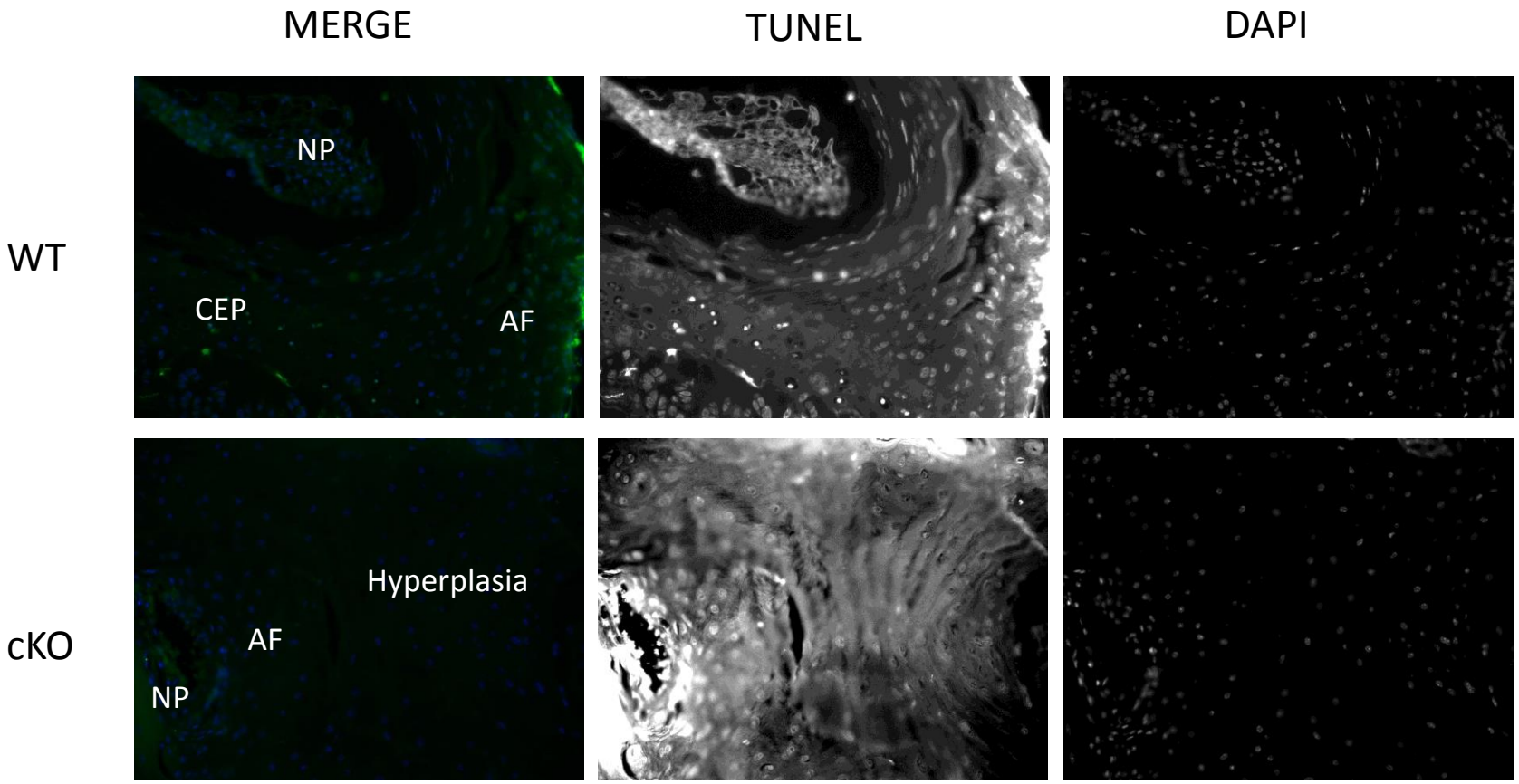

Fig S9

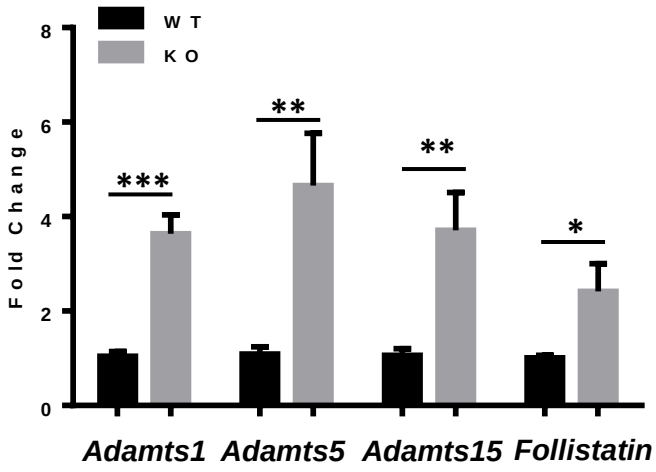
W T
K O
Fold Change
8
6
4
2
0
***
**
**
*
Adamts1
Adamts5
Adamts15
Follistatin

ID	gene_name	ADJ.P	PERIOD	LAG
ENSMUSG00000020917.11	Acly	8.79E-06	24	4
ENSMUSG00000038084.10	Opa1	9.81E-05	24	4
ENSMUSG00000020283.5	Pex13	9.81E-05	24	4
ENSMUSG00000009687.8	Fxyd5	0.000265	24	12
ENSMUSG00000027086.10	Fastkd1	0.000265	24	0
ENSMUSG00000046417.8	Fam211a	0.000265	24	2
ENSMUSG00000022053.7	Ebf2	0.000265	24	5
ENSMUSG00000047797.8	Gjb1	0.000265	24	16
ENSMUSG00000028989.3	Angptl7	0.000645	24	20
ENSMUSG00000025809.9	Itgb1	0.000645	24	4
ENSMUSG00000074766.4	Ism1	0.000645	24	3
ENSMUSG00000026643.10	Nmt2	0.000645	24	4
ENSMUSG00000019883.4	Echdc1	0.000645	24	4
ENSMUSG00000095512.1	Gm17222	0.000645	24	4
ENSMUSG00000047370.4	Gm7367	0.000645	24	12
ENSMUSG00000040605.6	Bace2	0.000645	24	4
ENSMUSG00000039956.2	Mrap	0.000645	24	4
ENSMUSG00000078234.5	Klhdc7a	0.000645	24	4
ENSMUSG00000073176.4	Zfp449	0.000645	24	4
ENSMUSG00000090305.1	Gm5459	0.000645	24	16
ENSMUSG00000029054.2	Gabrd	0.000645	24	2
ENSMUSG00000030972.5	Acsm5	0.001042	24	4
ENSMUSG00000021903.5	Galnt15	0.00144	24	20
ENSMUSG00000041607.10	Mbp	0.00144	24	18
ENSMUSG00000032010.8	Usp2	0.00144	24	22
ENSMUSG00000059824.4	Dbp	0.00144	24	18
ENSMUSG00000026922.7	Agpat2	0.00144	24	4
ENSMUSG00000041653.4	Pnpla3	0.00144	24	4
ENSMUSG00000026663.6	Atf6	0.00144	24	4
ENSMUSG00000029482.3	Aacs	0.00144	24	4
ENSMUSG00000090084.1	Srpx	0.00144	24	4
ENSMUSG00000039364.7	Sectm1b	0.00144	24	16
ENSMUSG00000051367.8	Six1	0.00144	24	6
ENSMUSG00000040370.7	Lyrm5	0.00144	24	2
ENSMUSG00000001700.9	Gramd3	0.00144	24	4
ENSMUSG00000031959.8	Wdr59	0.00144	24	2
ENSMUSG00000044645.7	Gm7334	0.00144	24	2
ENSMUSG00000025940.6	Tmem70	0.00144	24	4
ENSMUSG00000036225.8	Kctd1	0.00144	24	4
ENSMUSG00000021418.9	Rpp40	0.00144	24	2
ENSMUSG00000027663.6	Zmat3	0.00144	24	4
ENSMUSG00000031725.8	Ces1f	0.00144	24	4
ENSMUSG00000013523.7	Bcas1	0.00144	24	16
ENSMUSG00000073233.3	Gm9144	0.00144	24	16
ENSMUSG00000037016.7	Frem2	0.00144	24	4
ENSMUSG00000047473.8	Zfp30	0.00144	24	2
ENSMUSG00000025584.11	Pde8a	0.00144	24	4
ENSMUSG00000086432.1	B430119L08Rik	0.00144	24	6
ENSMUSG00000079168.3	Cd209g	0.00144	24	4

ENSMUSG00000074715.2	Ccl28		0.00144	24	4
ENSMUSG00000087235.1	Gm4750		0.00144	24	16
ENSMUSG00000044951.7	Mylk4		0.002993	24	22
ENSMUSG00000082476.1	Gm12242		0.002993	24	15
ENSMUSG00000076432.6	Ywhaq		0.002993	24	4
ENSMUSG00000063427.7	Rps10-ps2		0.002993	24	16
ENSMUSG00000040181.8	Fmo1		0.002993	24	2
ENSMUSG00000008540.5	Mgst1		0.002993	24	4
ENSMUSG00000021877.5	Arf4		0.002993	24	4
ENSMUSG00000029190.13	D5Ertd579e		0.002993	24	2
ENSMUSG00000036078.10	Sigmar1		0.002993	24	4
ENSMUSG00000022774.6	Ncbp2		0.002993	24	2
ENSMUSG00000027309.12	4930402H24Rik		0.002993	24	4
ENSMUSG00000022707.10	Gbe1		0.002993	24	4
ENSMUSG00000020777.10	Acox1		0.002993	24	2
ENSMUSG00000023832.7	Acat2		0.002993	24	3
ENSMUSG00000028567.8	Txndc12		0.002993	24	4
ENSMUSG00000023022.7	Lima1		0.002993	24	3
ENSMUSG00000039377.6	Hlx		0.002993	24	12
ENSMUSG00000041737.7	Tmem45b		0.002993	24	4
ENSMUSG00000020932.8	Gfap		0.002993	24	16
ENSMUSG00000021765.7	Fst		0.002993	24	4
ENSMUSG00000029208.10	Guf1		0.002993	24	2
ENSMUSG00000026749.5	Nek6		0.002993	24	2
ENSMUSG00000038517.9	Tbkbp1		0.002993	24	14
ENSMUSG00000005501.8	Usp40		0.002993	24	1
ENSMUSG00000020829.9	Slc46a1		0.002993	24	8
ENSMUSG00000094686.1	Ccl21a		0.002993	24	6
ENSMUSG00000073633.3	Fbxo36		0.002993	24	5
ENSMUSG00000027684.10	Mecom		0.002993	24	4
ENSMUSG00000052593.9	Adam17		0.002993	24	4
ENSMUSG00000040502.5		Mar-09	0.002993	24	2
ENSMUSG00000090659.2	Zfp493		0.002993	24	1
ENSMUSG00000040717.5	Il17rd		0.002993	24	4
ENSMUSG00000027792.5	Bche		0.002993	24	4
ENSMUSG00000054000.4	Tusc1		0.002993	24	14
ENSMUSG00000033182.6	Kbtbd12		0.002993	24	4
ENSMUSG00000037577.6	Ephx3		0.002993	24	4
ENSMUSG00000032517.9	Mobp		0.002993	24	16
ENSMUSG00000092746.2	Gm22179		0.002993	24	6
ENSMUSG00000028572.7	Hook1		0.002993	24	18
ENSMUSG00000029503.10	P2rx2		0.002993	24	16
ENSMUSG00000019890.3	Nts		0.00442	24	4
ENSMUSG00000029195.7	Klb		0.00442	24	4
ENSMUSG00000039099.7	Wdr93		0.00442	24	6
ENSMUSG00000037071.2	Scd1		0.005847	24	4
ENSMUSG00000025153.8	Fasn		0.005847	24	4
ENSMUSG00000021775.10	Nr1d2		0.005847	24	19
ENSMUSG00000030082.8	Sec61a1		0.005847	24	4
ENSMUSG00000021610.7	Clptm1l		0.005847	24	4

ENSMUSG00000022878.5	Adipoq	0.005847	24	4
ENSMUSG00000024286.7	Ccny	0.005847	24	2
ENSMUSG00000037470.8	Uggt1	0.005847	24	4
ENSMUSG00000009563.10	Tor2a	0.005847	24	4
ENSMUSG00000025007.7	Aldh18a1	0.005847	24	6
ENSMUSG00000022351.8	Sqle	0.005847	24	2
ENSMUSG00000028343.4	Erp44	0.005847	24	4
ENSMUSG00000060450.7	Rnf14	0.005847	24	2
ENSMUSG00000055116.7	Arntl	0.005847	24	6
ENSMUSG00000056973.6	Ces1d	0.005847	24	2
ENSMUSG00000047539.4	Fbxo28	0.005847	24	2
ENSMUSG00000028496.11	Mllt3	0.005847	24	2
ENSMUSG00000025981.7	Coq10b	0.005847	24	22
ENSMUSG00000069125.1	Rps24-ps2	0.005847	24	16
ENSMUSG00000031489.8	Adrb3	0.005847	24	4
ENSMUSG00000032724.5	Abtb2	0.005847	24	4
ENSMUSG00000001467.4	Cyp51	0.005847	24	3
ENSMUSG00000040564.7	Apoc1	0.005847	24	4
ENSMUSG00000003809.8	Gcdh	0.005847	24	2
ENSMUSG00000022131.2	Gpr180	0.005847	24	2
ENSMUSG00000004394.6	Tmed4	0.005847	24	2
ENSMUSG00000021666.10	Gfm2	0.005847	24	0
ENSMUSG00000041153.3	Osgin2	0.005847	24	2
ENSMUSG00000096795.1	Zfp433	0.005847	24	4
ENSMUSG00000015852.7	Fcrls	0.005847	24	4
ENSMUSG00000026181.11	Ppm1f	0.005847	24	4
ENSMUSG00000005069.6	Pex5	0.005847	24	0
ENSMUSG00000027341.4	Tmem230	0.005847	24	4
ENSMUSG00000030787.3	Lyve1	0.005847	24	2
ENSMUSG00000031358.11	Msl3	0.005847	24	4
ENSMUSG00000089682.3	Bcl2l2	0.005847	24	2
ENSMUSG00000029348.7	Asphd2	0.005847	24	4
ENSMUSG00000038180.5	Spag4	0.005847	24	5
ENSMUSG00000025102.8	3110040N11Rik	0.005847	24	2
ENSMUSG00000020038.9	Cry1	0.005847	24	4
ENSMUSG00000062480.5	Acat3	0.005847	24	4
ENSMUSG00000078923.4	Ube2v1	0.005847	24	14
ENSMUSG00000022074.5	Tnfrsf10b	0.005847	24	6
ENSMUSG00000027938.5	Creb3l4	0.005847	24	4
ENSMUSG00000097643.1	A130051J06Rik	0.005847	24	6
ENSMUSG00000024334.8	H2-Oa	0.005847	24	14
ENSMUSG00000096935.1	1700113A16Rik	0.005847	24	4
ENSMUSG00000002578.9	Ikzf4	0.005847	24	8
ENSMUSG00000034460.8	Six4	0.005847	24	4
ENSMUSG00000031910.8	Has3	0.005847	24	6
ENSMUSG00000040177.9	2310057M21Rik	0.005847	24	4
ENSMUSG00000005268.14	Prlr	0.005847	24	5
ENSMUSG00000073427.3	Gm4924	0.005847	24	2
ENSMUSG00000095969.1	Rnu1a1	0.005847	24	10
ENSMUSG00000074403.2	Hist2h3b	0.005847	24	11

ENSMUSG00000043687.9	1190005I06Rik	0.005847	24	4
ENSMUSG00000069208.5	Zfp825	0.005847	24	4
ENSMUSG00000083320.1	Gm13935	0.005847	24	20
ENSMUSG00000053038.7	Gm6180	0.005847	24	16
ENSMUSG00000044916.4	1700029I15Rik	0.005847	24	4
ENSMUSG00000081497.1	Gm15560	0.005847	24	16
ENSMUSG00000041930.7	Fam222a	0.005847	24	4
ENSMUSG00000097855.1	A930007I19Rik	0.008333	24	6
ENSMUSG00000040165.7	Cd209c	0.008333	24	4
ENSMUSG00000027762.5	Sucnr1	0.008333	24	4
ENSMUSG00000018865.8	Sult4a1	0.008333	24	14
ENSMUSG00000070436.5	Serpinh1	0.01082	24	4
ENSMUSG00000020585.4	Laptm4a	0.01082	24	4
ENSMUSG00000020889.11	Nr1d1	0.01082	24	16
ENSMUSG00000033022.7	Cdo1	0.01082	24	4
ENSMUSG00000024914.10	Drap1	0.01082	24	16
ENSMUSG00000032096.9	Arcn1	0.01082	24	4
ENSMUSG00000020532.12	Acaca	0.01082	24	4
ENSMUSG00000031701.5	Dnaja2	0.01082	24	0
ENSMUSG00000024538.7	Ppic	0.01082	24	4
ENSMUSG00000001494.6	Sost	0.01082	24	14
ENSMUSG00000046711.9	Hmga1	0.01082	24	14
ENSMUSG00000066632.2	Pgk1-rs7	0.01082	24	0
ENSMUSG00000032193.8	Ldlr	0.01082	24	3
ENSMUSG00000027879.3	Sec22b	0.01082	24	2
ENSMUSG00000061838.5	Suclg2	0.01082	24	0
ENSMUSG00000037379.4	Spon2	0.01082	24	7
ENSMUSG00000041891.9	Lman1	0.01082	24	4
ENSMUSG00000023827.2	Agpat4	0.01082	24	6
ENSMUSG00000029231.9	Pdgfra	0.01082	24	4
ENSMUSG00000019872.7	Smpdl3a	0.01082	24	4
ENSMUSG00000027088.4	Phospho2	0.01082	24	2
ENSMUSG00000031467.4	Agpat5	0.01082	24	2
ENSMUSG00000027742.8	Cog6	0.01082	24	2
ENSMUSG00000029009.11	Mthfr	0.01082	24	4
ENSMUSG00000063275.9	Ptpla	0.01082	24	4
ENSMUSG00000029685.9	Asb15	0.01082	24	22
ENSMUSG00000020471.5	Pold2	0.01082	24	13
ENSMUSG00000038416.8	Cdc16	0.01082	24	2
ENSMUSG00000035770.7	Dync1li2	0.01082	24	2
ENSMUSG00000029782.12	Tmem209	0.01082	24	16
ENSMUSG00000021916.9	Glt8d1	0.01082	24	3
ENSMUSG00000028955.3	Vamp3	0.01082	24	2
ENSMUSG00000024014.6	Pim1	0.01082	24	14
ENSMUSG00000034981.9	Parm1	0.01082	24	4
ENSMUSG00000026082.6	Rev1	0.01082	24	22
ENSMUSG00000031610.3	Scrg1	0.01082	24	2
ENSMUSG00000069631.8	Strada	0.01082	24	12
ENSMUSG00000027465.7	Tbc1d20	0.01082	24	4
ENSMUSG00000024150.5	Mcfd2	0.01082	24	2

ENSMUSG00000033453.7	Adamts15	0.01082	24	4
ENSMUSG00000024810.10	Il33	0.01082	24	2
ENSMUSG00000030545.8	Pex11a	0.01082	24	2
ENSMUSG00000031938.8	4931406C07Rik	0.01082	24	2
ENSMUSG00000021559.7	Dapk1	0.01082	24	4
ENSMUSG00000075486.3	Commd6	0.01082	24	3
ENSMUSG00000012422.8	Tmem167	0.01082	24	4
ENSMUSG00000074182.4	Znhit6	0.01082	24	22
ENSMUSG00000047554.7	Tmem41b	0.01082	24	4
ENSMUSG00000028293.8	Slc35a1	0.01082	24	4
ENSMUSG00000007777.3	0610009B22Rik	0.01082	24	5
ENSMUSG00000028256.10	Odf2l	0.01082	24	0
ENSMUSG00000075054.4	Yae1d1	0.01082	24	3
ENSMUSG00000039706.7	Ldb2	0.01082	24	5
ENSMUSG00000032018.7	Sc5d	0.01082	24	3
ENSMUSG00000034413.8	Neurl1b	0.01082	24	4
ENSMUSG00000019791.5	Hint3	0.01082	24	2
ENSMUSG00000097649.1	Gm10561	0.01082	24	4
ENSMUSG00000027555.8	Car13	0.01082	24	4
ENSMUSG00000046636.4	Gm7729	0.01082	24	16
ENSMUSG00000028990.7	Lzic	0.01082	24	2
ENSMUSG00000021567.8	Nkd2	0.01082	24	2
ENSMUSG00000070572.6	Trmt112-ps2	0.01082	24	14
ENSMUSG00000013646.11	Sh3bp5l	0.01082	24	1
ENSMUSG00000063439.6	B9d2	0.01082	24	16
ENSMUSG00000055917.8	Zfp277	0.01082	24	4
ENSMUSG00000039354.10	Smarcal1	0.01082	24	2
ENSMUSG00000060438.4	Rps10-ps1	0.01082	24	16
ENSMUSG00000089797.1	Gm16118	0.01082	24	18
ENSMUSG00000032346.7	Ooep	0.01082	24	4
ENSMUSG00000042340.5	Ctf1	0.01082	24	2
ENSMUSG00000073478.5	D730003I15Rik	0.01082	24	4
ENSMUSG00000020000.7	Moxd1	0.01082	24	4
ENSMUSG00000040321.3	Zfp770	0.01082	24	4
ENSMUSG00000043913.8	Ccdc60	0.01082	24	8
ENSMUSG00000096544.1	Gm4617	0.01082	24	15
ENSMUSG00000082530.1	Gm12168	0.01082	24	16
ENSMUSG00000030336.8	Cd27	0.01082	24	14
ENSMUSG00000015437.4	Gzmb	0.01082	24	13
ENSMUSG00000065824.1	Gm26315	0.01082	24	9
ENSMUSG00000046733.7	Gprc5a	0.01082	24	6
ENSMUSG00000041617.4	Ccdc74a	0.01082	24	8
ENSMUSG00000016181.4	Diexf	0.01082	24	4
ENSMUSG00000091803.1	Cox16	0.01082	24	2
ENSMUSG00000020407.7	Upp1	0.01082	24	6
ENSMUSG00000055137.6	5033411D12Rik	0.01082	24	4
ENSMUSG00000079343.3	Gm5077	0.01082	24	2
ENSMUSG00000037940.9	Inpp4b	0.01082	24	4
ENSMUSG00000039865.7	Slc44a3	0.01082	24	4
ENSMUSG00000039278.10	Pcsk1n	0.01082	24	16

ENSMUSG00000096862.1	Gm13301	0.01082	24	1
ENSMUSG00000079484.6	Phyhd1	0.01082	24	0
ENSMUSG00000097828.1	6430562O15Rik	0.01082	24	4
ENSMUSG00000025475.11	Gpr123	0.01082	24	7
ENSMUSG00000082088.1	Gm15753	0.01082	24	16
ENSMUSG00000086869.2	Gm7809	0.01082	24	0
ENSMUSG00000083567.2	Gm11451	0.01082	24	4
ENSMUSG00000041878.3	8430432A02Rik	0.01082	24	4
ENSMUSG00000074345.3	Tnfaip8l3	0.01082	24	4
ENSMUSG00000033615.9	Cplx1	0.01082	24	16
ENSMUSG00000048186.8	Bend7	0.01082	24	4
ENSMUSG00000081194.1	Gm8424	0.01082	24	4
ENSMUSG00000066438.6	Plekhd1	0.01082	24	16
ENSMUSG00000070577.5	Gm572	0.014955	24	4
ENSMUSG00000017300.9	Tnnc2	0.01909	24	18
ENSMUSG00000028618.5	Tmem59	0.01909	24	2
ENSMUSG00000035493.9	Tgfbi	0.01909	24	2
ENSMUSG00000036309.8	Skp1a	0.01909	24	1
ENSMUSG00000026509.10	Capn2	0.01909	24	2
ENSMUSG00000022816.5	Fstl1	0.01909	24	3
ENSMUSG00000079017.3	Ifi27l2a	0.01909	24	2
ENSMUSG00000008575.11	Nfib	0.01909	24	1
ENSMUSG00000030168.7	Adipor2	0.01909	24	4
ENSMUSG00000027605.12	Acss2	0.01909	24	4
ENSMUSG00000030774.7	Pak1	0.01909	24	20
ENSMUSG00000052837.5	Junb	0.01909	24	13
ENSMUSG00000019370.10	Calm3	0.01909	24	16
ENSMUSG00000022048.8	Dpysl2	0.01909	24	2
ENSMUSG00000027668.7	Mfn1	0.01909	24	0
ENSMUSG00000020893.11	Per1	0.01909	24	18
ENSMUSG00000030062.6	Rpn1	0.01909	24	0
ENSMUSG00000020817.10	Rabep1	0.01909	24	2
ENSMUSG00000022940.10	Pigp	0.01909	24	1
ENSMUSG00000020523.8	Fam114a2	0.01909	24	2
ENSMUSG00000042688.10	Mapk6	0.01909	24	9
ENSMUSG00000029390.7	Tmed2	0.01909	24	4
ENSMUSG00000081604.4	Gm11518	0.01909	24	14
ENSMUSG00000083899.2	Gm12346	0.01909	24	0
ENSMUSG00000052428.5	Tmco1	0.01909	24	4
ENSMUSG00000027131.3	Emc4	0.01909	24	3
ENSMUSG00000061731.3	Ext1	0.01909	24	4
ENSMUSG00000024370.10	Cdc23	0.01909	24	4
ENSMUSG00000045294.10	Insig1	0.01909	24	2
ENSMUSG00000044221.8	Grsf1	0.01909	24	1
ENSMUSG00000032998.10	Foxj3	0.01909	24	2
ENSMUSG00000071984.4	Fndc1	0.01909	24	4
ENSMUSG00000026585.7	Kifap3	0.01909	24	2
ENSMUSG00000025911.8	Adhfe1	0.01909	24	4
ENSMUSG00000016494.3	Cd34	0.01909	24	2
ENSMUSG00000030298.4	Sec13	0.01909	24	4

ENSMUSG00000022436.9	Sh3bp1	0.01909	24	14
ENSMUSG00000021417.8	Eci2	0.01909	24	4
ENSMUSG00000040928.9	S100pbp	0.01909	24	0
ENSMUSG00000029864.5	Gstk1	0.01909	24	4
ENSMUSG00000001962.8	Fam50a	0.01909	24	21
ENSMUSG00000005078.10	Jkamp	0.01909	24	4
ENSMUSG00000014402.8	Tsg101	0.01909	24	0
ENSMUSG00000031799.9	Tpm4	0.01909	24	4
ENSMUSG00000021756.6	Il6st	0.01909	24	2
ENSMUSG00000000194.7	Gpr107	0.01909	24	2
ENSMUSG00000055866.8	Per2	0.01909	24	22
ENSMUSG00000036940.9	Kdm1a	0.01909	24	2
ENSMUSG00000036099.10	Vezt	0.01909	24	11
ENSMUSG00000034893.7	Cog3	0.01909	24	0
ENSMUSG00000029474.6	Rnf34	0.01909	24	4
ENSMUSG00000024645.4	Timm21	0.01909	24	1
ENSMUSG00000051232.7	Tmem199	0.01909	24	4
ENSMUSG00000029554.9	Mad1l1	0.01909	24	16
ENSMUSG00000066233.5	Tmem42	0.01909	24	2
ENSMUSG00000027217.7	Tspan18	0.01909	24	4
ENSMUSG00000057789.7	Bak1	0.01909	24	12
ENSMUSG00000023992.8	Trem2	0.01909	24	16
ENSMUSG00000036513.9	Commd2	0.01909	24	22
ENSMUSG00000032030.10	Cul5	0.01909	24	4
ENSMUSG00000038936.7	Sccpdh	0.01909	24	2
ENSMUSG00000029759.3	Pon3	0.01909	24	3
ENSMUSG00000043635.6	Adamts3	0.01909	24	4
ENSMUSG00000040158.6	Tax1bp3	0.01909	24	2
ENSMUSG00000001300.9	Efnb2	0.01909	24	4
ENSMUSG00000026271.9	Gpr35	0.01909	24	10
ENSMUSG00000037001.10	Zfp39	0.01909	24	12
ENSMUSG00000049892.7	Rasd1	0.01909	24	4
ENSMUSG00000028369.9	Svep1	0.01909	24	2
ENSMUSG00000020653.5	Klf11	0.01909	24	14
ENSMUSG00000046731.3	Kctd11	0.01909	24	5
ENSMUSG00000035890.8	Rnf126	0.01909	24	8
ENSMUSG00000058729.7	Lin9	0.01909	24	17
ENSMUSG00000015971.4	Actr8	0.01909	24	2
ENSMUSG00000004356.7	Utp20	0.01909	24	0
ENSMUSG00000027313.3	Chac1	0.01909	24	16
ENSMUSG00000026482.7	Rgl1	0.01909	24	2
ENSMUSG00000036995.7	Asap3	0.01909	24	4
ENSMUSG00000086316.1	2210013O21Rik	0.01909	24	4
ENSMUSG00000069378.7	Prdm6	0.01909	24	6
ENSMUSG00000037669.8	1110057K04Rik	0.01909	24	2
ENSMUSG00000031533.3	Mrps31	0.01909	24	4
ENSMUSG00000025507.7	Lrdd	0.01909	24	14
ENSMUSG00000069255.6	Dusp22	0.01909	24	4
ENSMUSG00000030317.6	Timp4	0.01909	24	22
ENSMUSG00000007476.12	Lrrc8a	0.01909	24	4

ENSMUSG00000063889.10	Crem	0.01909	24	2
ENSMUSG00000037296.6	Lsm1	0.01909	24	4
ENSMUSG00000047182.5	Irs3	0.01909	24	4
ENSMUSG00000036819.8	Jmjd4	0.01909	24	11
ENSMUSG00000021339.3	Mrs2	0.01909	24	2
ENSMUSG00000020178.5	Adora2a	0.01909	24	6
ENSMUSG00000004500.8	Zfp324	0.01909	24	2
ENSMUSG00000034748.10	Sirt6	0.01909	24	10
ENSMUSG00000039033.5	Tasp1	0.01909	24	0
ENSMUSG00000033581.10	Igf2bp2	0.01909	24	4
ENSMUSG00000078897.4	Gm4724	0.01909	24	2
ENSMUSG00000007805.3	Twist2	0.01909	24	6
ENSMUSG00000039512.11	Uhrf1bp1	0.01909	24	4
ENSMUSG00000020354.9	Sgcd	0.01909	24	3
ENSMUSG00000097080.1	1700086O06Rik	0.01909	24	12
ENSMUSG00000030935.9	Acsm3	0.01909	24	4
ENSMUSG00000033825.9	Tpsb2	0.01909	24	4
ENSMUSG00000078249.4	Hmga1-rs1	0.01909	24	14
ENSMUSG00000049916.9	2610318N02Rik	0.01909	24	14
ENSMUSG00000053870.6	Fpgt	0.01909	24	4
ENSMUSG00000020151.10	Ptprr	0.01909	24	3
ENSMUSG00000081121.1	Gm12791	0.01909	24	17
ENSMUSG00000003062.8	Stard3nl	0.01909	24	0
ENSMUSG00000025221.9	Kcnip2	0.01909	24	4
ENSMUSG00000022206.6	Npr3	0.01909	24	2
ENSMUSG00000041762.10	Gpr155	0.01909	24	1
ENSMUSG00000057895.5	Zfp105	0.01909	24	1
ENSMUSG00000026048.10	Ercc5	0.01909	24	0
ENSMUSG00000074657.4	Kif5a	0.01909	24	16
ENSMUSG00000090215.2	Trim34b	0.01909	24	15
ENSMUSG00000043943.8	Naalad2	0.01909	24	4
ENSMUSG00000041020.8	Map7d2	0.01909	24	11
ENSMUSG00000050994.13	Adgb	0.01909	24	16
ENSMUSG00000030325.10	Klrb1c	0.01909	24	16
ENSMUSG00000036634.9	Mag	0.01909	24	16
ENSMUSG00000056592.8	Zfp658	0.01909	24	0
ENSMUSG00000028145.7	Them4	0.01909	24	4
ENSMUSG00000027001.4	Dusp19	0.01909	24	3
ENSMUSG00000086877.1	A230072C01Rik	0.01909	24	4
ENSMUSG00000097124.1	A530020G20Rik	0.01909	24	4
ENSMUSG00000078349.2	AW011738	0.01909	24	16
ENSMUSG00000031428.5	Zcchc18	0.01909	24	18
ENSMUSG00000044033.10	Ccdc141	0.01909	24	4
ENSMUSG00000041945.6	Mfsd9	0.01909	24	4
ENSMUSG00000042389.7	Tsen2	0.01909	24	4
ENSMUSG00000011751.10	Sptbn4	0.01909	24	17
ENSMUSG00000032556.9	Bfsp2	0.01909	24	16
ENSMUSG00000012187.7	Mogat1	0.01909	24	4
ENSMUSG00000092124.1	B930094E09Rik	0.01909	24	4
ENSMUSG00000024827.9	Gldc	0.01909	24	21

ENSMUSG00000081895.3	Gm10294		0.01909	24	20
ENSMUSG00000083859.1	Gm12003		0.01909	24	16
ENSMUSG00000059511.3	Gm20563		0.01909	24	4
ENSMUSG00000036095.10	Dgkb		0.01909	24	3
ENSMUSG00000055188.6	2900002K06Rik		0.01909	24	5
ENSMUSG00000087569.1	Gm8464		0.01909	24	16
ENSMUSG00000086670.1	Gm13194		0.01909	24	16
ENSMUSG00000061988.2	Rpl10a-ps2		0.01909	24	16
ENSMUSG00000031297.8	Slc7a3		0.01909	24	1
ENSMUSG00000049832.5	Gm9840		0.01909	24	18
ENSMUSG00000083668.1	Gm5648		0.01909	24	16
ENSMUSG00000035983.4	Gm7008		0.01909	24	16
ENSMUSG00000084941.1	Gm11944		0.01909	24	13
ENSMUSG00000033765.4	Calm4		0.01909	24	22
ENSMUSG00000040035.8	Disp2		0.01909	24	18
ENSMUSG00000034739.11	Mfrp		0.025686	24	4
ENSMUSG00000044948.10	Wdr96		0.025686	24	6
ENSMUSG00000049699.3	Ucn2		0.025686	24	16
ENSMUSG00000085893.1	Gm12091		0.032282	24	12
ENSMUSG00000022389.8	Tef		0.032282	24	21
ENSMUSG00000079037.3	Prnp		0.032282	24	3
ENSMUSG00000081992.1	Gm13408		0.032282	24	16
ENSMUSG00000021794.9	Glud1		0.032282	24	1
ENSMUSG00000030435.9	U2af2		0.032282	24	14
ENSMUSG00000031299.10	Pdha1		0.032282	24	1
ENSMUSG00000030058.11	Copg1		0.032282	24	2
ENSMUSG00000002257.7	Def6		0.032282	24	14
ENSMUSG00000049421.7	Zfp260		0.032282	24	2
ENSMUSG00000034902.11	Pip5k1c		0.032282	24	12
ENSMUSG00000041220.6	Elovl6		0.032282	24	3
ENSMUSG00000021748.8	Pdhb		0.032282	24	2
ENSMUSG00000030245.10	Golt1b		0.032282	24	4
ENSMUSG00000049760.5	2410015M20Rik		0.032282	24	4
ENSMUSG00000039100.9		Mar-06	0.032282	24	2
ENSMUSG00000014444.10	Piezo1		0.032282	24	8
ENSMUSG00000031770.9	Herpud1		0.032282	24	22
ENSMUSG00000022893.8	Adamts1		0.032282	24	2
ENSMUSG00000032116.11	Stt3a		0.032282	24	2
ENSMUSG00000037049.8	Smpd1		0.032282	24	2
ENSMUSG00000054690.11	Emcn		0.032282	24	3
ENSMUSG00000028150.8	Rorc		0.032282	24	2
ENSMUSG00000025511.8	Tspan4		0.032282	24	22
ENSMUSG00000029776.10	Hibadh		0.032282	24	1
ENSMUSG00000032563.9	Mrpl3		0.032282	24	3
ENSMUSG00000090266.4	Mettl23		0.032282	24	3
ENSMUSG00000026077.9	Npas2		0.032282	24	8
ENSMUSG00000025239.2	Limd1		0.032282	24	0
ENSMUSG00000017686.10	Rhot1		0.032282	24	2
ENSMUSG00000021395.10	Spin1		0.032282	24	1
ENSMUSG00000028149.6	Rap1gds1		0.032282	24	1

ENSMUSG00000038991.10	Txndc5	0.032282	24	2
ENSMUSG00000091512.1	Lamtor3	0.032282	24	2
ENSMUSG00000002017.9	Fam98a	0.032282	24	2
ENSMUSG00000032353.7	Tmed3	0.032282	24	2
ENSMUSG00000055319.7	Sec23ip	0.032282	24	0
ENSMUSG00000043252.8	Tmem64	0.032282	24	2
ENSMUSG00000063001.8	Rps23-ps	0.032282	24	0
ENSMUSG00000027367.10	Stard7	0.032282	24	0
ENSMUSG00000034064.8	Poglut1	0.032282	24	4
ENSMUSG00000002210.5	Smg9	0.032282	24	12
ENSMUSG00000095115.1	Itpripl2	0.032282	24	3
ENSMUSG00000016481.10	Cr1l	0.032282	24	0
ENSMUSG00000040374.7	Pex2	0.032282	24	3
ENSMUSG00000002949.8	Timm44	0.032282	24	4
ENSMUSG00000020114.6	Cand1	0.032282	24	0
ENSMUSG00000024269.5	Tpgs2	0.032282	24	3
ENSMUSG00000097971.2	Gm26917	0.032282	24	10
ENSMUSG00000020963.8	Tshr	0.032282	24	4
ENSMUSG00000036334.7	Igsf10	0.032282	24	4
ENSMUSG00000036782.7	Klhl13	0.032282	24	4
ENSMUSG00000001098.9	Kctd10	0.032282	24	2
ENSMUSG00000019874.5	Fabp7	0.032282	24	6
ENSMUSG00000030203.11	Dusp16	0.032282	24	0
ENSMUSG00000059689.8	Zfp637	0.032282	24	4
ENSMUSG00000037613.9	Tnfrsf23	0.032282	24	8
ENSMUSG00000027519.4	Rab22a	0.032282	24	3
ENSMUSG00000024778.6	Fas	0.032282	24	4
ENSMUSG00000035459.9	Stab2	0.032282	24	16
ENSMUSG00000020623.5	Map2k6	0.032282	24	20
ENSMUSG00000032705.8	Exd2	0.032282	24	1
ENSMUSG00000040659.3	Efhd2	0.032282	24	14
ENSMUSG00000048376.5	F2r	0.032282	24	4
ENSMUSG00000036646.7	Man1b1	0.032282	24	0
ENSMUSG00000026608.7	Kctd3	0.032282	24	4
ENSMUSG00000025241.9	Fyco1	0.032282	24	2
ENSMUSG00000025144.11	Stra13	0.032282	24	12
ENSMUSG00000034263.6	Vwa9	0.032282	24	4
ENSMUSG00000034300.10	Fam53c	0.032282	24	1
ENSMUSG00000067369.6	Trmt2b	0.032282	24	0
ENSMUSG00000066150.6	Slc31a1	0.032282	24	3
ENSMUSG00000017724.8	Etv4	0.032282	24	6
ENSMUSG00000028184.8	Lphn2	0.032282	24	5
ENSMUSG00000096173.1	Gm3150	0.032282	24	4
ENSMUSG00000015806.6	Qdpr	0.032282	24	0
ENSMUSG00000029125.8	Stx18	0.032282	24	4
ENSMUSG00000047777.9	Phf13	0.032282	24	2
ENSMUSG00000046532.7	Ar	0.032282	24	0
ENSMUSG00000038764.8	Ptpn3	0.032282	24	0
ENSMUSG00000039476.7	Prrx2	0.032282	24	5
ENSMUSG00000036932.8	Aifm1	0.032282	24	4

ENSMUSG00000052504.6	Epha3	0.032282	24	4
ENSMUSG00000087635.2	Gm13414	0.032282	24	16
ENSMUSG00000037762.6	Slc16a9	0.032282	24	6
ENSMUSG00000005907.8	Pex1	0.032282	24	3
ENSMUSG00000028024.8	Enpep	0.032282	24	8
ENSMUSG00000029815.7	Malsu1	0.032282	24	0
ENSMUSG00000064105.6	Cnnm2	0.032282	24	4
ENSMUSG00000028621.11	Cyb5rl	0.032282	24	4
ENSMUSG00000028152.4	Tspan5	0.032282	24	0
ENSMUSG00000070000.7	Fcho1	0.032282	24	14
ENSMUSG00000038816.8	Ctnnal1	0.032282	24	2
ENSMUSG00000039633.6	Lonrf1	0.032282	24	0
ENSMUSG00000032401.9	Lctl	0.032282	24	4
ENSMUSG00000026810.6	Dpm2	0.032282	24	8
ENSMUSG00000024277.8	Mapre2	0.032282	24	2
ENSMUSG00000036186.5	Fam69b	0.032282	24	4
ENSMUSG00000005225.9	Plekha8	0.032282	24	2
ENSMUSG00000029576.11	Radil	0.032282	24	4
ENSMUSG00000021646.8	Mccc2	0.032282	24	8
ENSMUSG00000024780.6	Cdc37l1	0.032282	24	2
ENSMUSG00000000148.11	Brat1	0.032282	24	4
ENSMUSG00000041406.8	BC055324	0.032282	24	16
ENSMUSG00000042487.5	Leo1	0.032282	24	6
ENSMUSG00000030763.6	Lcmt1	0.032282	24	22
ENSMUSG00000045410.11	Akr1e1	0.032282	24	2
ENSMUSG00000093392.1	Gm6061	0.032282	24	20
ENSMUSG00000029536.7	Gatc	0.032282	24	3
ENSMUSG00000017400.4	Stac2	0.032282	24	12
ENSMUSG00000030722.7	Nfatc2ip	0.032282	24	16
ENSMUSG00000044715.6	Gskip	0.032282	24	4
ENSMUSG00000093548.1	Gm6407	0.032282	24	15
ENSMUSG00000012126.10	Ubxn11	0.032282	24	11
ENSMUSG00000041650.9	Pcca	0.032282	24	1
ENSMUSG00000080875.2	Gm7332	0.032282	24	14
ENSMUSG00000031111.10	Igsf1	0.032282	24	6
ENSMUSG00000089764.1	Gm16580	0.032282	24	16
ENSMUSG00000071291.4	Zfp58	0.032282	24	6
ENSMUSG00000044636.5	Csrnp2	0.032282	24	4
ENSMUSG00000043122.6	A530016L24Rik	0.032282	24	2
ENSMUSG00000095675.1	Ccl21b	0.032282	24	5
ENSMUSG00000040164.3	Kcns1	0.032282	24	5
ENSMUSG00000037463.8	Fbxo27	0.032282	24	2
ENSMUSG00000022371.9	Col14a1	0.032282	24	2
ENSMUSG00000075318.6	Scn2a1	0.032282	24	5
ENSMUSG00000044122.8	Proca1	0.032282	24	2
ENSMUSG00000042505.6	Acn9	0.032282	24	2
ENSMUSG00000014782.9	Plekhg4	0.032282	24	8
ENSMUSG00000085738.2	Gm12335	0.032282	24	0
ENSMUSG00000046561.8	Arsj	0.032282	24	4
ENSMUSG00000028102.9	Pex11b	0.032282	24	2

ENSMUSG00000086679.1	Gm15551	0.032282	24	2
ENSMUSG00000037418.5	Best1	0.032282	24	4
ENSMUSG00000018500.2	Adora2b	0.032282	24	3
ENSMUSG00000091613.1	Gm17046	0.032282	24	4
ENSMUSG00000031482.8	Slc25a15	0.032282	24	0
ENSMUSG00000002083.6	Bbc3	0.032282	24	10
ENSMUSG00000070713.4	Gm10282	0.032282	24	14
ENSMUSG00000020396.8	Nefh	0.032282	24	16
ENSMUSG00000032593.5	Amigo3	0.032282	24	6
ENSMUSG00000047747.9	Rnf150	0.032282	24	20
ENSMUSG00000038583.6	Pln	0.032282	24	4
ENSMUSG00000042401.6	Crtac1	0.032282	24	14
ENSMUSG00000098495.1	RP24-113D21.1	0.032282	24	14
ENSMUSG00000047497.9	Adamts12	0.032282	24	0
ENSMUSG00000057157.3	Gm6054	0.032282	24	4
ENSMUSG00000092454.1	Gm2991	0.032282	24	14
ENSMUSG00000015002.10	Efr3a	0.032282	24	4
ENSMUSG00000028597.11	Gpx7	0.032282	24	2
ENSMUSG00000098198.1	Gm9169	0.032282	24	16
ENSMUSG00000079157.3	Fam155a	0.032282	24	0
ENSMUSG00000020599.7	Rgs9	0.032282	24	4
ENSMUSG00000097554.1	Gm26825	0.032282	24	22
ENSMUSG00000074398.5	Gm15441	0.032282	24	15
ENSMUSG00000095724.1	Gm21319	0.032282	24	20
ENSMUSG00000098985.1	RP24-570C10.6	0.032282	24	19
ENSMUSG00000081540.3	Gm12538	0.032282	24	3
ENSMUSG00000068165.2	Gm10233	0.032282	24	3
ENSMUSG00000005360.8	Slc1a3	0.032282	24	4
ENSMUSG00000062794.8	Zfp599	0.032282	24	12
ENSMUSG00000066270.2	Gm10157	0.032282	24	22
ENSMUSG00000045062.3	Pcdhb7	0.032282	24	6
ENSMUSG00000087433.1	Gm14167	0.032282	24	12
ENSMUSG00000081289.1	Gm14857	0.032282	24	15
ENSMUSG00000047307.1	Pcdhb13	0.032282	24	4
ENSMUSG00000027547.11	Sall4	0.032282	24	17
ENSMUSG00000086884.1	Gm16225	0.032282	24	16
ENSMUSG00000080775.1	Gm6368	0.032282	24	18
ENSMUSG00000033405.3	Nudt15	0.032282	24	3
ENSMUSG00000040904.4	Gm21988	0.032282	24	13
ENSMUSG00000029608.7	Rph3a	0.032282	24	17
ENSMUSG00000003410.7	Elavl3	0.032282	24	16
ENSMUSG00000062257.6	Opcml	0.032282	24	4
ENSMUSG00000035211.8	Xrra1	0.032282	24	6
ENSMUSG00000094248.1	Hist1h2ao	0.032282	24	15
ENSMUSG00000078087.4	Rps12l1	0.032282	24	22
ENSMUSG00000070271.5	Gm13268	0.032282	24	16
ENSMUSG00000062417.5	Hist1h3g	0.032282	24	12
ENSMUSG00000057626.1	Gm5621	0.032282	24	0
ENSMUSG00000082163.1	Gm14276	0.032282	24	12
ENSMUSG00000031995.2	St14	0.032282	24	16

ENSMUSG00000022144.3	Gdnf	0.042414	24	6
ENSMUSG00000030307.7	Slc6a11	0.042414	24	16
ENSMUSG00000009214.3	Tmem8c	0.042414	24	6
ENSMUSG00000034584.3	Exph5	0.042414	24	6
ENSMUSG00000044081.7	4930441O14Rik	0.042414	24	6
ENSMUSG00000036264.9	Fstl4	0.042414	24	18
ENSMUSG00000031376.9	Atp2b3	0.042414	24	5
ENSMUSG00000097760.1	6030442K20Rik	0.042414	24	4

The intervertebral disc contains intrinsic circadian clocks that are regulated by age and cytokines and linked to degeneration

Michal Dudek[1], Nan Yang[1], Jayalath PD Ruckshanthi[1], Jack Williams[1], Elzbieta Borysiewicz[1], Ping Wang[1], Antony Adamson[1], Jian Li[1], John F. Bateman[2], Michael R. White[1], Raymond P. Boot-Handford[3], Judith A Hoyland[4,5]*, Qing-Jun Meng[1,3]*

[1]Faculty of Life Sciences, University of Manchester, A.V.Hill Building, Oxford Road, Manchester, M13 9PT, UK.

[2]Murdoch Childrens Research Institute, Parkville, Victoria 3052, Australia.

[3]Wellcome Trust Centre for Cell Matrix Research, University of Manchester, Oxford Road, Manchester, M13 9PT, UK.
[4]Centre for Tissue Injury and Repair, Faculty of Medical and Human Sciences, University of Manchester, Stopford Building, Oxford Road, Manchester, M13 9PT.

[5]NIHR Manchester Musculoskeletal Biomedical Research Unit, Manchester Academic Health Science Centre, Manchester, UK

*Corresponding authors:

Dr. Qing-Jun Meng, Faculty of Life Sciences, University of Manchester, A.V.Hill Building, Oxford Road, Manchester, M13 9PT, UK. Email: qing-jun.meng@manchester.ac.uk Tel: +44 161 3068912.

Prof. Judith A Hoyland, Centre for Tissue Injury and Repair, Faculty of Medical and Human Sciences, University of Manchester, Stopford Building, Oxford Road, Manchester, M13 9PT. Email: judith.a.hoyland@manchester.ac.uk Tel: +44 161 2755425.

Running Title: IVD clock and degeneration

Key words: circadian clock, intervertebral disc, cytokine, ageing, *Bmal1*

Abstract

Objectives: The circadian clocks are internal timing mechanisms that drive ~24 hr rhythms in a tissue-specific manner. Many aspects of the physiology of the intervertebral disc (IVD) show clear diurnal rhythms. However, it is unknown whether IVD tissue contains functional circadian clocks and if so, how their dysregulation is implicated in IVD degeneration.

Methods: Clock gene dynamics in *ex vivo* IVD explants (from PER2::LUC reporter mice) and human disc cells (transduced with lentivirus containing *Per2*::luc reporters) were monitored in real-time by bioluminescence photon counting and imaging. Temporal gene expression changes were studied by RNAseq and qRT-PCR. IVD pathology was evaluated by histology in a mouse model with tissue-specific deletion of the core clock gene *Bmal1*.

Results: Here we show the existence of the circadian rhythm in mouse IVD tissue and human disc cells. This rhythm is dampened with ageing in mice and can be abolished by treatment with IL-1β but not TNFα. Time series RNAseq revealed 607 genes with 24 hr patterns of expression representing several essential pathways in IVD physiology. Mice with conditional knockout of *Bmal1* in their disc cells demonstrated age-related degeneration of IVDs.

Conclusions: We have established autonomous circadian clocks in mouse and human IVD cells which respond to age and cytokines, and control key pathways involved in the homeostasis of IVDs. Genetic disruption to the mouse IVD molecular clock predispose to IVD degeneration. These results support the concept that disruptions to circadian rhythms may be a risk factor for degenerative IVD disease and low back pain.

Introduction

The circadian clocks are internal timing mechanisms which drive ~24 hr rhythms in physiology and behaviour. In mammals, the central pacemaker Suprachiasmatic Nuclei (SCN) in the hypothalamus synchronizes peripheral clocks in most major body organs.[1-3] Circadian rhythms coordinate tissue-specific physiology with light/darkness, rest/activity feeding cycles and body temperature fluctuations.[1 4] Disruptions to circadian rhythms (during ageing or in shift workers) have been linked to increased risk of diseases (e.g. obesity, diabetes, cardiovascular disease, and osteoarthritis.[5 6] At the molecular level, the circadian clock consists of a network of transcriptional activators (*Clock*, *Bmal1*) and repressors (*Per1/2* and *Cry1/2*) organized in a negative feedback loop.[6] This core oscillator generates 24 hour rhythms in the expression of not only its core components but also a myriad of clock controlled genes (CCGs). Depending on the tissue, expression of 3-16% of the whole transcriptome exhibits a circadian rhythm.[7]

The spine is comprised of bony vertebral bodies alternating with fibro-cartilagenous intervertebral discs (IVD). IVD degeneration is among the most prevalent musculoskeletal disorders affecting one in five people under 60 and more than half of the people above 60 years of age.[8] Low back pain, which is often associated with IVD degeneration, is the number one cause of Years Lived with Disability in the developed countries.[9] Existing evidence suggests that the IVD is a highly rhythmic tissue, experiencing a diurnal cycle of higher loading (activity phase),[10 11] followed by a period of low-load recovery (resting phase). Under high load the pressurized interstitial fluid flows to regions of lower pressure through the outer annulus fibrosus (AF) and the cartilaginous end plate (CEP), resulting in decreased disc height, AF outward bulging and an increase in osmolarity of the central gelatinous nucleus pulposus (NP). During the recovery period, the process is reversed by high osmotic pressure inside the disc causing fluid flow to the NP.[12] Exchange of nutrients/metabolites that occurs with fluid flow during this cycle maintains disc cell homeostasis.[13]

Consistent with the rhythmic nature of IVD tissue, shift work (a factor known to disrupt circadian rhythms) was reported to be associated with higher risk of LBP and IVD degeneration.[14-18] We have previously shown that environmental disruption of circadian rhythm in mice, when combined with high fat diet, leads to degeneration of the lumbar IVD tissue in mice.[19] More recently, changes in the expression of circadian clock genes have been identified in rat IVD tissues following passive smoking (a risk factor for LBP).[20] However, no studies have examined whether IVD cells express intrinsic circadian clocks, how these IVD clocks are regulated, what their targets are, and whether genetic disruption to the IVD clock impact on tissue homeostasis and susceptibility to degeneration.

In this study, we systemically characterized the molecular circadian clock mechanisms in mouse and human IVD tissue/cells. Moreover, by generating a tissue-specific *Bmal1* KO mouse model, our study provides the first genetic evidence linking a core clock factor to IVD degeneration.

Results

Intervertebral disc possesses a functional, temperature entrainable circadian clock

To test whether the IVD contains a molecular circadian clock capable of driving circadian rhythm of gene expression we monitored the dynamics of PER2::Luc protein in IVD explant cultures isolated from PER2::Luc reporter mice.[21] Real-time bioluminescence photon counting demonstrated robust circadian rhythm of PER2::Luc activity which lasted for more than 5 days, with a period of 23.93 +/- 0.10 hrs (mean +/- SEM, n=6, Fig. 1A). As the IVD comprises two distinct cell types, the NP and AF cells, we wanted to know if both regions exhibit circadian rhythms. Live imaging of the mouse IVD explants using high sensitivity EM-CCD camera revealed rhythmic PER2::Luc signals from both AF and NP cells (see Supplementary videos 1-3). To extend these studies to humans, primary human NP cells were transiently transfected with a vector carrying the luciferase gene under the control of the *Per2* promoter. This approach revealed cell autonomous circadian oscillations of *Per2::luc* expression, indicating the operation of a functional clock machinery in these human disc cells (Fig. 1B). IHC staining of human NP tissue sections using antibodies against BMAL1 and CLOCK confirmed presence of these essential circadian clock components in human discs (Fig. 1C).

One of the key properties of a peripheral circadian clock is their ability to respond to time cues that are controlled by the SCN clock, such as hormones or changes in body temperature. Since the IVDs are not vascularised or innervated (except in pathological conditions)[22], we hypothesised that daily body temperature oscillations may be a mechanism of clock entrainment for IVDs. To test this, IVD explants from the same mouse were placed in different incubators programmed to have oppositely phased cyclic temperature changes for 4 days (38.5°C for 12 hrs/35.5°C for 12 hrs, or vice versa), before returning to a constant 37°C. As a control, another IVD explant from the same mouse was incubated under constant 37°C. The PER2::Luc rhythms in IVD explants were all in similar circadian phase for the first 3 days before the temperature protocol (Fig. 1D). Once the antiphasic protocol was introduced, the oscillations were driven 180 ° out of phase with each other. Interestingly, the antiphasic oscillations were maintained for at least three more days after the tissues were released to constant temperature. In contrast, the IVD explant that remained at constant temperature gradually lost its ability to oscillate by day 7, mainly due to desynchronization in culture (Fig. 1D). These results clearly indicate that temperature cycles that approximate body temperature changes are capable of not only entraining the circadian phase of the IVD oscillation, but enhancing the oscillation amplitude.

Aging affects the circadian rhythm of IVDs

Daily systemic time cues in body temperature and hormone release are known to be altered with aging.[23] In addition, intrinsic properties of the clock oscillator could deteriorate with age as well.[23] [24] Indeed, we have previously demonstrated that the amplitude of circadian oscillations in cartilage and tendon tissues dampen with aging.[25] [26] Therefore, we hypothesized that circadian rhythms may change in aging disc, compromising the daily control of IVD physiology. To assess this, we compared the oscillations of PER2::Luc expression in mouse IVD explant cultures from animals aged 2 and 12 months (Fig. 2A, supplementary Video 1). The amplitude of oscillations in IVDs from 12 months old mice was severely reduced (by ~60%) as compared to 2 month old mice. Additionally, the average period of oscillations was significantly lengthened by 1.6 hrs in IVDs from 12 month old mice (Fig. 2A). IHC staining showed decreased expression of the core circadian transcription factors BMAL1 and CLOCK in 12 month (Fig. S1) and 24 month old mice as compared to 2

month old (Fig. 2B). These data demonstrate that the IVD clock becomes dysregulated with ageing.

The circadian rhythm of IVD is disrupted by IL-1β in a NF-κB dependent manner

Chronic inflammation is a known factor associated with IVD degeneration and lower back pain.[27] To investigate the effects of catabolic cytokines on disc circadian clock, we treated IVD explants from the PER2::Luc reporter mice with IL-1β, LPS and TNFα. Tissues were under continuous bioluminescence recording. Treatment with IL-1β (or LPS, Fig. S2A) resulted in complete disruption of the PER2::Luc circadian rhythm, associated with significant changes of clock genes (*Bmal1, Per2* and *Nr1d1*)(Fig. 3A, Fig.S3). The disrupted rhythm could be reinstated by ~~the addition of~~ dexamethasone (an anti-inflammatory glucocorticoid, Fig. 3A) or IL-1RA (an antagonist of IL-1, Fig.S2B), but not by forskolin (a clock synchronising agent without anti-inflammatory properties, Fig. ~~S2B~~S2C). NFκB is one of the classic pathways through which IL-1β can mediate its effects. To evaluate the involvement of NFκB, we used the IKK1/2 inhibitor BMS-345541 to block the activation of NFκB. The clock-disrupting effect of IL-1β was blocked by pre-treating the IVD explant with BMS-345541, supporting a role of NFκB pathway in the IL-1β -mediated clock disruption. In contrast to IL-1β, treatment of IVD explants with TNFα had no effect on their circadian rhythms (Fig. 3B). In contrast, both IL-1β and TNFα elicited a strong induction of NFκB signalling in a lung epithelial cell line, suggesting a possible cell-type specific response (Fig.S2D). Next, we took advantage of a transgenic mouse strain expressing the p65-DsRedXP protein fusion construct[28] to observe the nuclear translocation of p65, one of the major components of the NFκB complex. Live imaging showed that treatment of IVD explants with IL-1β caused rapid nuclear translocation of p65 both in AF and NP cells. However, addition of TNFα (up to 40 ng/mL) had no effect on p65 translocation (Fig.3C).

There are at least two potential mechanisms through which IL-1β could disrupt the IVD circadian rhythm. Individual cells may still have robust clocks but become desynchronised, with their clocks being in different phases, leading to reduced oscillation amplitude; or individual cells may have lost their pacemaking properties. To distinguish between these two possibilities, we used a high sensitivity EM-CCD camera to visualize the PER2::Luc bioluminescence signals from individual cells in the presence or absence of IL-1β. Consistent with the lack of effect of forskolin, this imaging approach revealed loss of bioluminescence at single cell level, excluding the desynchronization hypothesis (Fig. 3D and Supplementary video 2). Therefore, disruption to the IVD clock could be a hitherto undiscovered response to pro-inflammatory cytokines.

Identification of the first IVD circadian transcriptome

Circadian clocks in different tissues exert their local functions through regulating diverse yet highly tissue-specific set of target genes. To reveal the extent of rhythmic genes in IVD tissue under physiological conditions, we performed a time-series RNAseq study using IVD tissues (collected every 4 hours for 48 hours) from mice kept in 12 hr light/12 hr darkness. We used a well-recognized JTKCycle[29] algorithm to pick out rhythmic genes. Using P_{adjust}<0.05 as a cut-off, we identified 607 genes (3.5% of expressed genes in IVD) with rhythmic 24 hr expression patterns (Figure 4A, Supplementary Table 1). Further phase

Formatted: Font: Italic

Formatted: Font: Italic

clustering analysis of these rhythmic genes using R package revealed 4 main clusters (Fig. ~~S3~~S4), with more than 70% of these genes peaking at night time points (representing the active phase of mouse). Gene ontology (GO)-term analysis using topGO revealed dozens of overrepresented functional groups with an adjusted p< 0.01, including "fatty acid metabolic process", "circadian rhythm", "intracellular protein transmembrane transport", "intrinsic apoptotic signaling pathway", "carboxylic acid metabolic process", and "response to endoplasmic reticulum stress". We next compared the IVD rhythmic gene list to that of the mouse cartilage and tendon we published earlier.[25 26] There was a very small number of genes (6-16%) overlapping between any two of these skeletal tissues, with only 16 genes common to all three, supporting the tissue-specific function of the peripheral clocks (Figure 4B). Of these 16 common genes, 8 were core circadian clock genes. The expression profiles of canonical clock genes (*Bmal1*, *Per2, Dbp*) and selected target genes *Follistatin* (a BMP antagonist)[30] *and Timp4* (a tissue inhibitor of MMPs)[31] relevant to IVD physiology and catabolism were validated by temporal qRT-PCR in mouse IVD tissues (Figure 4C, Fig~~ure~~ S4~~5~~).

Targeted deletion of *Bmal1* causes age-dependent IVD degeneration

Bmal1 is an essential circadian clock component for the generation of 24 hr rhythms. The global *Bmal1* knock-out mouse shows multi-tissue pathologies, including ectopic calcification of IVDs.[32] However, the severe disruption to whole body circadian rhythms confounds interpretation of phenotype. To evaluate the function of local IVD clocks, we produced a conditional KO mouse model (Col2a1-*Bmal1* KO, cKO) with a cell type-specific abolition of the transcription factor *Bmal1* in α1(II) collagen expressing cells, including NP and AF cells, and chondrocytes.[33] We have previously shown that the central SCN clock and behavioural locomotion rhythms in the cKO mice are not affected.[33] IHC staining of IVDs confirmed loss of BMAL1 expression in the majority of the AF cells and chondrocytes of the cartilaginous end plate in cKO mice (Fig. 5A). The cKO mouse was crossed with the PER2::Luc mouse to enable real-time tracking of clock rhythms. Photon counting of PER2::Luc bioluminescence demonstrated a lack of circadian oscillations in the cKO IVDs, with no response to dexamethasone treatment (Fig. 5B). Bioluminescence imaging of the cKO IVDs confirmed lack of circadian oscillations of PER2::Luc in both AF and NP cells (Fig. 5C and Supplementary video 3).

Histological analysis revealed early signs of degeneration of the lumbar IVDs in cKO mouse at 6 months of age, such as thinning of the growth plate of vertebral body (Fig. 6A), and gradual disappearance of the CEP (Fig. ~~S4~~S~~5~~6). At 12 months, there was widespread degeneration of lumbar IVDs in cKOs. Bone bridges appeared within the growth plate, the CEP was almost completely replaced by bone (Fig. 6A, black arrow), and the height of the disc was significantly reduced in cKO IVDs (Fig. 6A). In addition, staining with Safranin O and picrosirius red revealed disorganisation of the outer annulus structure and signs of fibrosis (with organized collagen bundles) appearing at the periphery of the IVDs (Fig. 6A-C, asterisk). Finally, using X-ray studies, the cKO mice showed clear signs of calcification and narrowing of spaces between vertebrae at 6 months (in tail IVDs, data not shown) and 12 months (in lumbar IVDs, Fig. 6C~~, red and yellow arrows~~). No signs of degeneration were evident in age-matched WT mice up to the age of 12 months (Fig. 6B). However, similar degenerative changes to the cKO mutants were visible in WT mice at 24 months of age (Fig. ~~S5~~S~~6~~7), suggesting the possibility that loss of *Bmal1* and/or circadian rhythm in IVD cells

leads to accelerated ageing of the tissue. TUNEL assay and qPCR were performed to explore the underlying mechanisms for the observed phenotype. There were no obvious signs of apoptosis, although significant upregulation of catabolism-related genes (*Adamts1, Adamts5, Adamts15* and *Follistatin*) were observed in cKO IVDs (Fig.S8, S9). Together, these results indicate the essential role of the locally expressed core clock factor BMAL1 in IVD homeostasis, loss of which led to profound tissue degeneration.

Discussion

Low back pain is amongst the most prevalent spinal diseases associated with increasing age, with over 80% of the UK population predicted to experience back pain within their lifetime. Progressive degeneration of the IVD tissue, partly caused by increased catabolism driven by inflammatory/catabolic cytokines, is a major contributing factor in LBP.[34] It has long been known that the physiology of IVD is under strong influence by a diurnal rhythm associated with the rest/activity cycles, i.e., daily cycles of loading (activity phase) and low-load recovery (resting phase).[10-13] Exchange of nutrients/metabolites that occurs with fluid flow during this cycle maintains disc cell homeostasis. Recent epidemiological and experimental studies have linked shift work (in humans) and chronic disruption of circadian rhythms (in mice) to higher risk of IVD degeneration.[14 15 17-19] However, our study represents the first critical analysis of the molecular and cellular mechanisms of the IVD clock under physiological and pathological conditions. Using the clock gene reporter mouse/cell models, as well as a conditional *Bmal1* KO mouse model that had disrupted IVD clock, we established autonomous circadian clocks in mouse and human IVD cells that respond to temperature cycles, dampen with age and become dysregulated by catabolic cytokines. Genetic disruption to the mouse IVD molecular clock predisposes to IVD degeneration. Global *Bmal1* KO also showed a phenotype in the skeletal system, including the spine. However, our conditional KO model allows us to conclude the essential role of locally expressed BMAL1 or circadian rhythm in maintaining IVD homeostasis. These results support the notion that disruptions to circadian rhythms during ageing or in shift workers may be a contributing factor for the increased susceptibility to degenerative IVD diseases and low back pain.

Formatted: Font: Italic

We also revealed for the first time the circadian transcriptome of the IVD tissue. Of particular interest are the genes and pathways that have been previously implicated in IVD physiology and pathology, such as genes involved in matrix homeostasis/repair (e.g Follistatin, Timp4, Adamts1, Adamts5, Adamts15 and Adam17),[30 31] mitochondria function and fatty acid metabolism (e.g. Pex1, Pex2, Pex5, Pex15, Adipoq, Adipor2, Fasn).[35 36] Although glucose and anaerobic glycolysis represent major metabolic pathways in IVD, there is evidence that mitochondria in the NP are functional and they retain the capacity to metabolise fatty acids through mitochondrial oxidative metabolism.[35] Other relevant pathways include ER stress and apoptosis (e.g. Aifm1, Atf6, Chac1, Bak1, Bbc3, Opa1 and Fas).[37 38] The diverse clock-controlled pathways identified by this approach implicate circadian rhythm as a critical regulatory mechanism for IVD biology.

Using IVD tissue explants, we have identified the disruption of the circadian clock in IVD as hitherto undiscovered response to pro-inflammatory cytokines. Similar clock disruptions by

inflammatory cytokines have been found in other cell types, such as in macrophages,[39] synovial fibroblasts,[40] and chondrocytes.[28] The involvement of NFκB pathway in mediating the effects of IL-1 is consistent with our earlier findings in chondrocytes, where NFκB interferes with the core clock complex to disrupt circadian pacemaking.[28] Given the diverse pathways controlled by the IVD clock, cytokine-mediated circadian disruption may be involved in driving key aspects of the catabolic response of IVD to chronic inflammation. Therefore, there is the possibility of stabilizing IVD clock rhythm as a novel strategy to combat tissue catabolism. Although the concentration we used for IL-1β (5 ng/mL) in these tissue explant studies was higher than that in degenerative IVD (~50 pg/mL), this dose is in line with most *ex vivo*/*in vitro* studies.

We also identified a lack of response of the IVD clock (and cartilage clock)[28] to TNFα, possibly due to the defective NFκB nuclear translocation. These findings suggest IL-1 and TNFα may act on distinct downstream pathways and regulate different target genes within the IVD, as seen in chondrocytes. In SW1353 chondrocyte-derived cells, catabolic genes such as IL-6, BMP-2, MMP13 and COX-2 only respond to IL-1, with almost no response to TNFα.[41 42] Such results are intriguing because we have shown that IL-1β plays a more prominent role in driving disc degeneration than TNFα.[43 44] Therefore, anti-inflammatory drugs that selectively target IL-1 are more likely to bring therapeutic benefits.

In conclusion, our results provide a firm basis for future studies that aim to elucidate the functional implication and therapeutic potential of the human IVD circadian rhythm in health and disease of the spine.

References

1 Hastings MH, Reddy AB, Maywood ES. A clockwork web: circadian timing in brain and periphery, in health and disease. *Nat Rev Neurosci* 2003;4(8):649-61.
2 Partch CL, Green CB, Takahashi JS. Molecular architecture of the mammalian circadian clock. *Trends Cell Biol* 2014;24(2):90-9.
3 Reppert SM, Weaver DR. Coordination of circadian timing in mammals. *Nature* 2002;418(6901):935-41.
4 Bass J, Takahashi JS. Circadian integration of metabolism and energetics. *Science* 2010;330(6009):1349-54.
5 Dudek M, Meng QJ. Running on time: the role of circadian clocks in the musculoskeletal system. *Biochem J* 2014;463(1):1-8.
6 Takahashi JS, Hong HK, Ko CH, *et al*. The genetics of mammalian circadian order and disorder: implications for physiology and disease. *Nat Rev Genet* 2008;9(10):764-75.
7 Zhang R, Lahens NF, Ballance HI, *et al*. A circadian gene expression atlas in mammals: implications for biology and medicine. *Proc Natl Acad Sci USA* 2014;111(45):16219-24.
8 Boden SD, Davis DO, Dina TS, *et al*. Abnormal magnetic-resonance scans of the lumbar spine in asymptomatic subjects. A prospective investigation. *J Bone Joint Surg Am* 1990;72(3):403-8.
9 Global Burden of Disease Study C. Global, regional, and national incidence, prevalence, and years lived with disability for 301 acute and chronic diseases and injuries in 188 countries, 1990-2013: a systematic analysis for the Global Burden of Disease Study 2013. *Lancet* 2015;386(9995):743-800.

10 Haschtmann D, Stoyanov JV, Ferguson SJ. Influence of diurnal hyperosmotic loading on the metabolism and matrix gene expression of a whole-organ intervertebral disc model. *J Orthop Res* 2006;24(10):1957-66.
11 Malko JA, Hutton WC, Fajman WA. An in vivo magnetic resonance imaging study of changes in the volume (and fluid content) of the lumbar intervertebral discs during a simulated diurnal load cycle. *Spine* 1999;24(10):1015-22.
12 Matsumoto T, Kawakami M, Kuribayashi K, *et al*. Cyclic mechanical stretch stress increases the growth rate and collagen synthesis of nucleus pulposus cells in vitro. *Spine* 1999;24(4):315-9.
13 van der Veen AJ, van Dieen JH, Nadort A, *et al*. Intervertebral disc recovery after dynamic or static loading in vitro: is there a role for the endplate? *J Biomech* 2007;40(10):2230-5.
14 Elfering A, Semmer N, Birkhofer D, *et al*. Risk factors for lumbar disc degeneration: a 5-year prospective MRI study in asymptomatic individuals. *Spine* 2002;27(2):125-34.
15 Kaila-Kangas L, Kivimaki M, Harma M, *et al*. Sleep disturbances as predictors of hospitalization for back disorders-a 28-year follow-up of industrial employees. *Spine* 2006;31(1):51-6.
16 Leino-Arjas P, Kaila-Kangas L, Kauppinen T, *et al*. Occupational exposures and inpatient hospital care for lumbar intervertebral disc disorders among Finns. *Am J Ind Med* 2004;46(5):513-20.
17 Rajaratnam SM, Arendt J. Health in a 24-h society. *Lancet* 2001;358(9286):999-1005.
18 Zhao I, Bogossian F, Turner C. The effects of shift work and interaction between shift work and overweight/obesity on low back pain in nurses: results from a longitudinal study. *J Occup Environ Med* 2012;54(7):820-5.
19 Kc R, Li X, Forsyth CB, Voigt RM, *et al*. Osteoarthritis-like pathologic changes in the knee joint induced by environmental disruption of circadian rhythms is potentiated by a high-fat diet. *Sci Rep* 2015;5:16896.
20 Numaguchi S, Esumi M, Sakamoto M, *et al*. Passive cigarette smoking changes the circadian rhythm of clock genes in rat intervertebral discs. *J Orthop Res* 2016;34(1):39-47.
21 Yoo SH, Yamazaki S, Lowrey PL, *et al*. PERIOD2::LUCIFERASE real-time reporting of circadian dynamics reveals persistent circadian oscillations in mouse peripheral tissues. *Proc Natl Acad Sci USA* 2004;101(15):5339-46.
22 Freemont AJ, Peacock TE, Goupille P, *et al*. Nerve ingrowth into diseased intervertebral disc in chronic back pain. *Lancet* 1997;350(9072):178-81.
23 Brown SA, Pagani L, Cajochen C, *et al*. Systemic and cellular reflections on ageing and the circadian oscillator: a mini-review. *Gerontology* 2011;57(5):427-34.
24 Davidson AJ, Yamazaki S, Arble DM, *et al*. Resetting of central and peripheral circadian oscillators in aged rats. *Neurobiol Aging* 2008;29(3):471-7.
25 Gossan N, Zeef L, Hensman J, *et al*. The circadian clock in murine chondrocytes regulates genes controlling key aspects of cartilage homeostasis. *Arthritis Rheum* 2013;65(9):2334-45.
26 Yeung CY, Gossan N, Lu Y, *et al*. Gremlin-2 is a BMP antagonist that is regulated by the circadian clock. *Sci Rep* 2014;4:5183.
27 Molinos M, Almeida CR, Caldeira J, *et al*. Inflammation in intervertebral disc degeneration and regeneration. *J R Soc Interface* 2015;12(108):20150429.
28 Guo B, Yang N, Borysiewicz E, *et al*. Catabolic cytokines disrupt the circadian clock and the expression of clock-controlled genes in cartilage via an NFsmall ka, CyrillicB-dependent pathway. *Osteoarthritis Cartilage* 2015;23(11):1981-8.
29 Hughes ME, Hogenesch JB, Kornacker K. JTK_CYCLE: an efficient nonparametric algorithm for detecting rhythmic components in genome-scale data sets. *J Biol Rhythms* 2010;25(5):372-80.

30 McMahon JA, Takada S, Zimmerman LB, *et al*. Noggin-mediated antagonism of BMP signaling is required for growth and patterning of the neural tube and somite. *Genes Dev* 1998;12(10):1438-52.
31 Vo NV, Hartman RA, Yurube T, *et al*. Expression and regulation of metalloproteinases and their inhibitors in intervertebral disc aging and degeneration. *Spine J* 2013;13(3):331-41.
32 Bunger MK, Walisser JA, Sullivan R, *et al*. Progressive arthropathy in mice with a targeted disruption of the Mop3/Bmal-1 locus. *Genesis* 2005;41(3):122-32.
33 Dudek M, Gossan N, Yang N *et al*. The chondrocyte clock gene Bmal1 controls cartilage homeostasis and integrity. *J Clin Invest* 2016;126(1):365-76.
34 Luoma K, Riihimaki H, Luukkonen R, *et al*. Low back pain in relation to lumbar disc degeneration. *Spine* 2000;25(4):487-92.
35 Agrawal A, Guttapalli A, Narayan S, *et al*. Normoxic stabilization of HIF-1alpha drives glycolytic metabolism and regulates aggrecan gene expression in nucleus pulposus cells of the rat intervertebral disk. *Am J Physiol Cell Physiol* 2007;293(2):C621-31.
36 Rannou F, Lee TS, Zhou RH, *et al*. Intervertebral disc degeneration: the role of the mitochondrial pathway in annulus fibrosus cell apoptosis induced by overload. *Am J Pathol* 2004;164(3):915-24.
37 Lee HW, Kim SY, Kim AY, *et al*. Adiponectin stimulates osteoblast differentiation through induction of COX2 in mesenchymal progenitor cells. *Stem cells* 2009;27(9):2254-62.
38 Wang H, Liu H, Zheng ZM, *et al*. Role of death receptor, mitochondrial and endoplasmic reticulum pathways in different stages of degenerative human lumbar disc. *Apoptosis* 2011;16(10):990-1003.
39 Spengler ML, Kuropatwinski KK, Comas M, *et al*. Core circadian protein CLOCK is a positive regulator of NF-kappaB-mediated transcription. *Proc Natl Acad Sci USA* 2012;109(37):E2457-65.
40 Haas S, Straub RH. Disruption of rhythms of molecular clocks in primary synovial fibroblasts of patients with osteoarthritis and rheumatoid arthritis, role of IL-1beta/TNF. *Arthritis Res Ther* 2012;14(3):R122.
41 Shi J, Schmitt-Talbot E, DiMattia DA, *et al*. The differential effects of IL-1 and TNF-alpha on proinflammatory cytokine and matrix metalloproteinase expression in human chondrosarcoma cells. *Inflamm Res* 2004;53(8):377-89.
42 Tetlow LC, Adlam DJ, Woolley DE. Matrix metalloproteinase and proinflammatory cytokine production by chondrocytes of human osteoarthritic cartilage: associations with degenerative changes. *Arthritis Rheum* 2001;44(3):585-94.
43 Hoyland JA, Le Maitre C, Freemont AJ. Investigation of the role of IL-1 and TNF in matrix degradation in the intervertebral disc. *Rheumatology* 2008;47(6):809-14.
44 Le Maitre CL, Hoyland JA, Freemont AJ. Catabolic cytokine expression in degenerate and herniated human intervertebral discs: IL-1beta and TNFalpha expression profile. *Arthritis Res Ther* 2007;9(4):R77.
45 Storch KF, Paz C, Signorovitch J, *et al*. Intrinsic circadian clock of the mammalian retina: importance for retinal processing of visual information. *Cell* 2007;130(4):730-41.
46 Sakai K, Hiripi L, Glumoff V, *et al*. Stage-and tissue-specific expression of a Col2a1-Cre fusion gene in transgenic mice. *Matrix Biol* 2001;19(8):761-7.
47 Sladek M, Rybova M, Jindrakova Z, *et al*. Insight into the circadian clock within rat colonic epithelial cells. *Gastroenterology* 2007;133(4):1240-9.
48 J AAaR. topGO: topGO: Enrichment analysis for Gene Ontology. R package version 2.22.0. 2010.
49 J K. Rtsne: T-Distributed Stochastic Neighbor Embedding using Barnes-Hut Implementation, 2015.
50 Sive JI, Baird P, Jeziorsk M, *et al*. Expression of chondrocyte markers by cells of normal and degenerate intervertebral discs. *Mol Pathol* 2002;55(2):91-7.

Figure legends

Figure 1. IVDs possess an autonomous circadian clock. (A) Representative PER2::Luc bioluminescence trace of mouse IVD explant culture (period = 23.93 ± 0.247h; mean ± SD; n=6); (B) Representative trace of human NP cells transduced with a *Per2::luc* reporter (period=22.52 ± 0.39h; mean ± SD; n=3); (C) IHC of BMAL1 and CLOCK on NP biopsy of human IVDs (magnification 5x left, 10x right); n=3. (D) Temperature entrainment (n=4). Two IVD explant cultures (represented by red and blue traces) from the same animal were held under antiphase temperature cycles (alternating 12-hour cycles of 38.5°C/35.5°C; baseline temperature= 37°C). Third IVD explant culture from the same animal was kept at a constant temperature of 37°C (Purple trace below).

Figure 2. Circadian rhythm of IVD is dampened during aging. (A) Representative bioluminescence traces of young (2 months) and ageing (12 months) IVDs from PER2::Luc mice. The period was significantly lengthened in older mice ($p<0.05$) and the amplitude was significantly dampened ($p<0.05$) (two-tailed nonparametric Mann-Whitney test; n=4); (B) IHC of BMAL1 and CLOCK on young (3 months) and aged (24 months) mouse IVDs; n=4. Magnification 10x. The Safranin O staining panel on the right was included to ease visualization of the different structures of the IVD. NP- nucleus pulposus; AF- annulus fibrosus; OAF- outer annulus fibrosus; CEP- cartilaginous end plate.

Figure 3. IL-1β, but not TNFα, disrupts the circadian rhythm of IVDs. (A) Representative bioluminescence traces of PER2::Luc mouse IVD explants. Arrows indicate time of treatment with IL-1β (5 ng/mL), IKK inhibitor (BMS-345541, 10 μM) and dexamethasone (100 nM). Red trace - treated with IL-1β, green trace - pre-treated with IKK inhibitor before addition of IL-1β, blue trace - vehicle control; n=3. (B) Representative bioluminescence traces treated with TNFα (red trace, 40 ng/mL) or control (blue trace). Arrows indicate time of treatments; n=3. (C) Live fluorescence imaging of p65DsRed reporter in mouse IVDs by confocal microscopy before and after treatment with IL-1β or TNFα. Scale bar 20 μm. Arrows indicate the nuclei. AF- annulus fibrosus; NP- nucleus pulposus; (D) Live bioluminescence imaging of an IVD tissue from PER2::Luc mouse, treated with IL-1β (at 48h), followed by dexamethasone (at 96h).

Formatted: Font: 11 pt

Figure 4. Circadian transcriptome in mouse IVD identified by time series RNA sequencing. (A) Heat map depicting the expression patterns of the 607 rhythmic genes (3.5 % of the IVD transcriptome) identified by JTKCycle. Genes were organized according to timing of peak expression. White bars represent the day; black bars represent the night. (B) Venn diagram comparing the number of rhythmic genes of IVD, cartilage and tendon. (C) qPCR validation of time-dependent expression of clock genes (*Bmal1, Per2* and *Dbp)* and target genes (*Follistatin* and *Timp4*) in mouse IVDs normalized to *Gapdh*. Mean and SEM (n = 6). Grey shadow indicates the night phase.

Figure 5. Conditional deletion of *Bmal1* in *Col2a1*-expressing cells results in disruption of the circadian rhythms in mouse IVDs. (A) IHC of BMAL1 in 3 month old WT and KO mice (magnification: upper panels 10x and lower panels 40x); n=3. (B) Representative bioluminescence traces of WT (blue) and *Bmal1* cKO (red) mouse IVD explant cultures; n=6. Arrow indicates treatment with dexamethasone. (C) Live

bioluminescence imaging of IVDs from WT and *Bmal1* cKO IVDs from mice on a PER2::Luc background.

Figure 6. Loss of *Bmal1* leads to degeneration of IVDs and cartilaginous tissues of the spine. (A) Safranin O staining of 12 month old WT and *Bmal1* cKO mouse lumbar IVDs; n=4. Red arrow-loss of CEP; Black arrow- fragmentation of growth plate; *-fibrosis (magnification 2.5x). Analysis of the IVD height and growth plate thickness was shown (two-tailed nonparametric Mann-Whitney test; n=4) *- p<0.05; *** - p<0.001. (B) Picrosirius red staining of lumbar IVDs from 12 month old WT and *Bmal1* cKO mouse showing organisation of collagen (magnification 2.5x left and 5x right panels); n=4. Images were visualized under brightfield or polarized light. (C) X-ray radiography of 12 month old WT and *Bmal1* cKO mouse spines; n=3. Yellow arrows- calcification of IVDs; Red arrows- calcification of tissues surrounding the IVDs.

Supplementary figure legends

Figure S1. Reduced expression of BMAL1 and CLOCK in ageing IVDs. IHC of BMAL1 and CLOCK on sections of IVDs from 3 and 12 months old mice; n=4. Magnification, 5x left and middle panels, 10x right panels. BMAL1 staining was visible in the AF, but not the CEP, of 12 month old mice. CLOCK staining was largely absent in both AF and CEP in 12 month old mice.

Figure S2. Effects of LPS, IL-1RA ~~and,~~ forskolin and TNFα on IVD oscillations. Representative bioluminescence traces of PER2::Luc mouse IVD explants; n=3. (A) LPS treatment (1 μg/mL, red trace) disrupted the rhythm, which could be rescued by treatment with dexamethasone (100 nM). (B, C) Disrupted circadian rhythm by IL-1β treatment (5 ~~μg~~ng/mL, red trace) was not rescued by application of forskolin (10 μM), but by pre-treatment with IL-1RA (1 μg/mL)~~could not be rescued by forskolin, a clock synchronising agent~~. Arrows indicate time of treatment. (D) Both IL-1β (5 ng/mL) and TNFα (40 ng/mL) induced strong NFκB signalling in lung epithelial cells stably transfected with NFκB::luc reporter. Representative, n=3.

Figure S3. Effects of IL-1β on endogenous clock gene expression. qPCR of several clock genes, *Adamts1* and *IL-6* in IVD explants upon IL-1β treatment (5 ng/mL for 4 hours). *, p<0.05; ***, p<0.001, n=4.

Figure ~~S3~~S4. Phase clustering analysis of rhythmic genes in mouse IVDs. Clustering analysis was performed using cluster (A) and Rtsne (B) of R package. These analyses revealed 4 main clusters with different peak times (two at night and two during the day). Example genes for each cluster were highlighted. There was a good concordance between these two methods of analysis.

Figure ~~S4~~S5. Time course qPCR of *β-actin* in mouse IVDs. Note the lack of circadian rhythms. Mean and SEM (n = 6).

Formatted: Font: Bold
Formatted: Font: Italic
Formatted: Font: Italic
Formatted: Font: Bold
Formatted: Font: Bold, Italic
Formatted: Font: Bold

Figure S6. Early onset of IVD degeneration in IVDs from 6 month old cKO mice. Safranin O/methyl green staining revealed gradual disappearance of CEP in the *Bmal1* cKO mouse (black arrow); n=4.

Figure ~~S5~~S7. Spontaneous degeneration of IVDs from aged WT mice. Picrosirius red staining and polarised light microscopy were performed on IVDs from 3 and 24 month old wild type mice; n=4. The aged WT mouse IVDs display a phenotype similar to *Bmal1* cKO IVDs, with fibrosis of the outer AF composed of bundles of organised collagen visible under polarised light microscope.

Figure S8. TUNEL staining of IVDs from 12 months old WT and *Bmal1* cKO mice. Note there were no detectable signs of apoptosis in either WT or cKO IVDs. N=4.

Figure S9. Time course qPCR of catabolic genes in IVDs from 3 months old WT and *Bmal1* cKO mice. Mean and SEM (n = 4). *, p<0.05; **, p<0.01; ***, p<0.001.

Formatted: Font: Bold
Formatted: Font: Not Bold
Formatted: Font: Not Bold
Formatted: Font: Not Italic

Supplementary table and videos

Supplementary Table 1. List of rhythmic IVD genes with a ~24 hr period.

Supplementary Video 1, Live bioluminescence imaging of the PER2::Luc mouse IVD explants (2 month on the left and 12 month on the right) using high sensitivity EM-CCD camera.

Supplementary Video 2, Live bioluminescence imaging of the PER2::Luc mouse IVD explants treated with IL-1β (at 48 hr), followed by Dex (at 96 hr).

Supplementary Video 3, Live bioluminescence imaging of the mouse IVD explants from a WT mouse (left) and a *Bmal1* cKO mouse (right).

Supplementary Online Methods

Animals

All animal studies were performed in accordance with the 1986 UK Home Office Animal Procedures Act. Approval was provided by the local ethics committee. Mice were maintained at 20-22°C, with standard rodent chow available *ad libitum* and under 12:12 hr light dark schedule (light on at 7 am; light off at 7 pm). *Bmal1*$^{flox/flox}$ mice[45] were crossed onto a PER2::luc background. The PER2::Luc mice carry the firefly luciferase gene fused in-frame with the 3' end of the *Per2* gene, creating a fusion protein reporter.[21] *Bmal1*$^{flox/flox}$ - PER2::Luc mice were subsequently crossed with *Col2a1*^{cre} mice expressing cre recombinase under the control of the *Col2a1* promoter[46] to generate cartilage/IVD specific *Bmal1* KO. All mice were bred in-house at the University of Manchester. Genotyping of the *Col2a1-Bmal1*$^{-/-}$ mice was described before.[33]

Reagents and antibodies

IL-1β and TNFα were purchased from R&D, lipopolysaccharides (LPS), BMS-345541, dexamethasone (Dex), Forskolin (FSK) were purchased from Sigma. The following antibodies were used in this study, BMAL1 (mouse monoclonal)[47] and CLOCK (Abcam ab3517).

Tissue explant cultures, bioluminescence recording and imaging

Organotypic IVD tissue explants were prepared as described before.[28] Explants were cultured on 0.4-µm cell culture inserts (Millipore), and bioluminescence was recorded in real time using a LumiCycle apparatus (Actimetrics). Baseline subtraction was carried out using a 24-hour moving average. Amplitude was measured at second peak from the start of recording and period was determined from three peaks using LumiCycle analysis software. For temperature entrainment the incubator housing the LumiCycle after 37°C three day initial phase were set to oscillate the temperature from to 35.5°C for 12 hours to 38.5°C for 12 hours for four cycles. Another incubator was cycling the temperature in opposite phase. Third incubator was kept at constant 37°C temperature as control.

For live tissue bioluminescence imaging, intervertebral discs of the WT and *Col2a1-Bmal1*$^{-/-}$ mice (on a PER2::Luc background) were imaged using a self-contained Olympus Luminoview LV200 microscope (Olympus) and recorded using a cooled Hamamatsu ImageEM C9100-13 EM-CCD camera.[33] Images were taken every hour for the duration of the experiment and combined in ImageJ.

Time course sample collections, mRNA extraction, RNAsequencing and quantitative real-time PCR

The circadian transcriptome studies in mouse IVD were performed as described before.[25] Intervertebral discs were obtained from 8-12 weeks old mice kept under 12 hr/12 hr light/darkness conditions. IVDs were collected every 4 hr for 48 hrs, starting at 9 am (zeitgeber time ZT2). 3-4 lumbar discs of the same animal were pooled to obtain sufficient material. The tissues were immediately snap frozen in liquid nitrogen, and then stored at -80°C until mRNA extraction. Tissues were homogenised using a Mikro-Dismembrator S (Satorius Stedim Biotech) with the barrel and ball of the dismembrator pre-cooled in liquid nitrogen. mRNA was extracted using RNeasy micro kit (Qiagen) according to the manufacturer's protocol. Quality and integrity of total RNA samples were assessed using a 2100 Bioanalyzer or a 2200 TapeStation (Agilent Technologies) according to the manufacturer's instructions. Thus prepared mRNA was used for RNAseq and qPCR analysis.

For RNA sequencing, RNA-seq libraries were generated using the TruSeq® Stranded mRNA assay (Illumina, Inc.) according to the manufacturer's protocol. Briefly, total RNA (0.1-4 µg) was used as input material from which polyadenylated mRNA was purified using poly-T, oligo-attached, magnetic beads. The mRNA was then fragmented using divalent cations under elevated temperature and then reverse transcribed into first strand cDNA using random primers. Second strand cDNA was then synthesised using DNA Polymerase I and RNase H. Following a single 'A' base addition, adapters were ligated to the cDNA fragments, and the products then purified and enriched by PCR to create the final cDNA library. Adapter indices were used to multiplex libraries, which were pooled prior to cluster generation using a cBot instrument. The loaded flow-cell was then paired-end sequenced (101 + 101 cycles,

plus indices) on an Illumina NextSeq instrument. Demultiplexing of the output data (allowing one mismatch) and BCL-to-Fastq conversion was performed with CASAVA 1.8.3. 101bp×101bp paired-end reads were generated from each sample. Up to 82M total reads were obtained in each sample.

For qPCR, RNA concentrations were determined using NanoDrop 2000 (Thermo Scientific), equal amounts of RNA were converted to cDNA using the High Capacity cDNA Reverse Transcription (RT) Kit (Applied Biosystems). Taqman based qPCR was carried out using a StepOne Plus Real-Time PCR System (Applied Biosystems) with Fast Blue qPCR MasterMix (Eurogentec). Taqman primers and probes were purchased from Applied Biosystems. Gene names and probe IDs are as follows, *Gapdh*: Mm99999915_g1; *Arntl*, Mm00500226_m1; *Per2*, Mm00478113_m1; *Dbp*, Mm01194021_m1; *Follistatin*, Mm00514982_m1; *Timp4*, Mm01184417_m1.

Bioinformatic analysis of the RNAseq data

The fastq files were analysed with FastQC and any low quality reads and contaminated barcodes were trimmed with Trimmomactic. All libraries were aligned to GRCm38.p2 assembly of mouse genome using Tophat-2.1.0 and only matches with the best score were reported for each read. The mapped reads were counted by genes with HTSeq against gencode.vM2.annotation.gtf. Genes with very low expressed (with average read across all time point <10) were filtered out. Time-dependent genes were identified by JTKCycle.[29] The rhythmic genes with a 24 hr period and an adjusted p value less than 0.05 were selected for further validation. GO analysis of the JTK_CYCLE identified circadian genes was performed using topGO of the R package.[48] These genes were also clustered with cluster and Rtsne of the R package.[49] Raw data were deposited in EMBL-EBI Array Express (accession number pending).

Human tissues and cells and lentiviral transduction

Adult human IVD specimens were obtained with informed consent from the Intervertebral Disc Tissue Bank at the University of Manchester, using surgical specimens from patients undergoing disc surgery for treatment of disc herniation or IVD degeneration, in accordance with local ethical committee approval. Tissue was processed for cell extraction and representative samples of all tissues containing intact AF and NP regions were formalin-fixed, paraffin-embedded and sections histologically graded as previously reported[50] with samples graded as follows: non-degenerate (grade 0-4); mildly degenerate (grade 5-7); and severely degenerate (grade 8-12). Only low grade samples (grade 0-2) were used in this study. NP tissue from each sample was macroscopically dissected from AF, and finely minced prior to enzymatic digestion in a solution of 0.1% (w/v) type II collagenase and 0.1% (w/v) hyaluronidase in serum-free DMEM overnight at 37°C with agitation. Isolated cells were cultured in DMEM supplemented with 10% (v/v) FBS, 1 mM sodium pyruvate, 10,000U/ml penicillin, 10mg/ml streptomycin, 25µg/ml amphotericin B and 1mM ascorbate under standard conditions (37°C, 21% O_2, 5% CO_2). Cells were then expanded in monolayer and used at passage <2. Grade 2 cells were used for *Per2::luc* lentiviral transduction and bioluminescence photon counting.

Lentiviral transduction of primary human NP cells was performed using methods previously described.[25] Briefly, lentiviral particles containing a *Per2*::luc reporter were produced in HEK 293T packaging cells and used to transduce the human NP cells. Cells were then synchronized with forskolin before lumicycle recording.

Histology and immunohistochemistry

Mouse spines were dissected and fixed in PBS 4% paraformaldehyde solution followed by decalcification in 20% EDTA pH 7.4. Decalcified tissues were processed and embedded in paraffin. Frontally embedded lumbar spine paraffin blocks were sectioned on a microtome to 5 µm thickness, 3-4 sections per slide. Each block yielded 40-50 slides. Every 5th slide was stained with Saffranin O and the sections were examined for the presence of disc degeneration. H&E, picrosirius red and Safranin O staining were performed according to standard protocols. Safranin O stained sections were imaged using Zeiss Observer D1 Axiocam 105 color camera and measurements of disc height and growth plate thickness were performed in ImageJ. Picrosirius red stained slides were imaged under brightfield or polarized light. The latter allows us to incorporate the birefringent properties of fibrillar collagen, in order to visualize the more organized collagen molecules.

IHC was performed using DAB staining method as described previously.[25] Briefly, the slides were deparaffinised and rehydrated. Antigen retrieval was performed using 1mg/mL Trypsin in PBS (Sigma) digestion for 10 min. Slides were washed and blocked with blocking solution (3% donkey serum in PBS TritonX 0.1%) for 1 h at room temperature. The slides were then incubated with primary antibody diluted in blocking solution overnight at 4°C. Subsequently slides were washed and incubated with fluorescent secondary antibody diluted in blocking solution for 1 h at 4°C. One of the sections on each slide was used as no primary antibody control.

Live imaging of p65-DsRed

Intervertebral discs from p65-DsRed mouse were cut in half to expose both the AF and NP tissue and embedded in the Matrigel matrix (BD Biosciences) in 35-mm glass bottom Cellview dishes (Greiner Bio-one). Images were acquired with a Zeiss LSM 780 Confocal Inverted Microscope in a humidified CO_2 incubator (at 37°C, 5% CO_2) with a C-Apochromat 40×/1.2 W Korr objective. During imaging tissue was treated with IL-1β (5–20 ng/mL) or TNFα (up to 40 ng/mL). DsRedXP tagged p65 was visualized by excitation with a green helium neon laser (543 nm) and detection through both a 545-nm dichroic mirror and a 560-nm long pass filter. Data capture was performed using ZEN2010B software (Zeiss).

Statistical analysis

Data were evaluated using Two-tailed Student's *t*-test, two way ANOVA or non-parametric, two-tailed Mann-Whitney test. Results were presented as mean ± SEM from at least three independent experiments. Differences were considered significant at the values of *P < 0.05, **P < 0.01 and ***P < 0.001.

Funding
This work was funded by a Medical Research Council (MRC) UK Career Development Award (G0900414, to Q.J. Meng); an Arthritis Research UK Senior Research Fellowship Award (20875, to Q.J. Meng); an MRC project grant (MR/K019392/1, to Q.J. Meng and R.P. Boot-Handford); a Wellcome Trust (UK) Core funding grant (088785/Z/09/Z) to the University of Manchester Wellcome Trust Centre for Cell Matrix Research. Consumables for processing of human IVD and isolation and culture of human IVD cells were funded by the National Institute for Health Research Manchester Musculoskeletal Biomedical Research Unit. The Funders had no role in the study design, data interpretation, report and submission of this work.

Supplementary Online Methods

Animals

All animal studies were performed in accordance with the 1986 UK Home Office Animal Procedures Act. Approval was provided by the local ethics committee. Mice were maintained at 20-22°C, with standard rodent chow available *ad libitum* and under 12:12 hr light dark schedule (light on at 7 am; light off at 7 pm). *Bmal1*$^{flox/flox}$ mice[45] were crossed onto a PER2::luc background. The PER2::Luc mice carry the firefly luciferase gene fused in-frame with the 3' end of the *Per2* gene, creating a fusion protein reporter.[21] *Bmal1*$^{flox/flox}$ - PER2::Luc mice were subsequently crossed with *Col2a1*^{cre} mice expressing cre recombinase under the control of the *Col2a1* promoter[46] to generate cartilage/IVD specific *Bmal1* KO. All mice were bred in-house at the University of Manchester. Genotyping of the *Col2a1-Bmal1*$^{-/-}$ mice was described before.[33]

Reagents and antibodies

IL-1β and TNFα were purchased from R&D, lipopolysaccharides (LPS), BMS-345541, dexamethasone (Dex), Forskolin (FSK) were purchased from Sigma. The following antibodies were used in this study, BMAL1 (mouse monoclonal)[47] and CLOCK (Abcam ab3517).

Tissue explant cultures, bioluminescence recording and imaging

Organotypic IVD tissue explants were prepared as described before.[28] Explants were cultured on 0.4-μm cell culture inserts (Millipore), and bioluminescence was recorded in real time using a LumiCycle apparatus (Actimetrics). Baseline subtraction was carried out using a 24-hour moving average. Amplitude was measured at second peak from the start of recording and period was determined from three peaks using LumiCycle analysis software. For temperature entrainment the incubator housing the LumiCycle after 37°C three day initial phase were set to oscillate the temperature from to 35.5°C for 12 hours to 38.5°C for 12 hours for four cycles. Another incubator was cycling the temperature in opposite phase. Third incubator was kept at constant 37°C temperature as control.

For live tissue bioluminescence imaging, intervertebral discs of the WT and *Col2a1-Bmal1*$^{-/-}$ mice (on a PER2::Luc background) were imaged using a self-contained Olympus Luminoview LV200 microscope (Olympus) and recorded using a cooled Hamamatsu ImageEM C9100-13 EM-CCD camera.[33] Images were taken every hour for the duration of the experiment and combined in ImageJ.

Time course sample collections, mRNA extraction, RNAsequencing and quantitative real-time PCR

The circadian transcriptome studies in mouse IVD were performed as described before.[25] Intervertebral discs were obtained from 8-12 weeks old mice kept under 12 hr/12 hr light/darkness conditions. IVDs were collected every 4 hr for 48 hrs, starting at 9 am (zeitgeber time ZT2). 3-4 lumbar discs of the same animal were pooled to obtain sufficient material. The tissues were immediately snap frozen in liquid nitrogen, and then stored at -80°C until mRNA extraction. Tissues were homogenised using a Mikro-Dismembrator S (Satorius Stedim Biotech) with the barrel and ball of the dismembrator pre-cooled in liquid

nitrogen. mRNA was extracted using RNeasy micro kit (Qiagen) according to the manufacturer's protocol. Quality and integrity of total RNA samples were assessed using a 2100 Bioanalyzer or a 2200 TapeStation (Agilent Technologies) according to the manufacturer's instructions. Thus prepared mRNA was used for RNAseq and qPCR analysis.

For RNA sequencing, RNA-seq libraries were generated using the TruSeq® Stranded mRNA assay (Illumina, Inc.) according to the manufacturer's protocol. Briefly, total RNA (0.1-4 μg) was used as input material from which polyadenylated mRNA was purified using poly-T, oligo-attached, magnetic beads. The mRNA was then fragmented using divalent cations under elevated temperature and then reverse transcribed into first strand cDNA using random primers. Second strand cDNA was then synthesised using DNA Polymerase I and RNase H. Following a single 'A' base addition, adapters were ligated to the cDNA fragments, and the products then purified and enriched by PCR to create the final cDNA library. Adapter indices were used to multiplex libraries, which were pooled prior to cluster generation using a cBot instrument. The loaded flow-cell was then paired-end sequenced (101 + 101 cycles, plus indices) on an Illumina NextSeq instrument. Demultiplexing of the output data (allowing one mismatch) and BCL-to-Fastq conversion was performed with CASAVA 1.8.3. 101bp×101bp paired-end reads were generated from each sample. Up to 82M total reads were obtained in each sample.

For qPCR, RNA concentrations were determined using NanoDrop 2000 (Thermo Scientific), equal amounts of RNA were converted to cDNA using the High Capacity cDNA Reverse Transcription (RT) Kit (Applied Biosystems). Taqman based qPCR was carried out using a StepOne Plus Real-Time PCR System (Applied Biosystems) with Fast Blue qPCR MasterMix (Eurogentec). Taqman primers and probes were purchased from Applied Biosystems. Gene names and probe IDs are as follows, *Gapdh*: Mm99999915_g1; *Arntl*, Mm00500226_m1; *Per2*, Mm00478113_m1; *Dbp*, Mm01194021_m1; *Follistatin*, Mm00514982_m1; *Timp4*, Mm01184417_m1.

Bioinformatic analysis of the RNAseq data

The fastq files were analysed with FastQC and any low quality reads and contaminated barcodes were trimmed with Trimmomactic. All libraries were aligned to GRCm38.p2 assembly of mouse genome using Tophat-2.1.0 and only matches with the best score were reported for each read. The mapped reads were counted by genes with HTSeq against gencode.vM2.annotation.gtf. Genes with very low expressed (with average read across all time point <10) were filtered out. Time-dependent genes were identified by JTKCycle.[29] The rhythmic genes with a 24 hr period and an adjusted p value less than 0.05 were selected for further validation. GO analysis of the JTK_CYCLE identified circadian genes was performed using topGO of the R package.[48] These genes were also clustered with cluster and Rtsne of the R package.[49] Raw data were deposited in EMBL-EBI Array Express (accession number pending).

Human tissues and cells and lentiviral transduction

Adult human IVD specimens were obtained with informed consent from the Intervertebral Disc Tissue Bank at the University of Manchester, using surgical specimens from patients undergoing disc surgery for treatment of disc herniation or IVD degeneration, in accordance

with local ethical committee approval. Tissue was processed for cell extraction and representative samples of all tissues containing intact AF and NP regions were formalin-fixed, paraffin-embedded and sections histologically graded as previously reported[50] with samples graded as follows: non-degenerate (grade 0-4); mildly degenerate (grade 5-7); and severely degenerate (grade 8-12). Only low grade samples (grade 0-2) were used in this study. NP tissue from each sample was macroscopically dissected from AF, and finely minced prior to enzymatic digestion in a solution of 0.1% (w/v) type II collagenase and 0.1% (w/v) hyaluronidase in serum-free DMEM overnight at 37°C with agitation. Isolated cells were cultured in DMEM supplemented with 10% (v/v) FBS, 1 mM sodium pyruvate, 10,000U/ml penicillin, 10mg/ml streptomycin, 25µg/ml amphotericin B and 1mM ascorbate under standard conditions (37°C, 21% O_2, 5% CO_2). Cells were then expanded in monolayer and used at passage <2. Grade 2 cells were used for *Per2::luc* lentiviral transduction and bioluminescence photon counting.

Lentiviral transduction of primary human NP cells was performed using methods previously described.[25] Briefly, lentiviral particles containing a *Per2*::luc reporter were produced in HEK 293T packaging cells and used to transduce the human NP cells. Cells were then synchronized with forskolin before lumicycle recording.

Histology and immunohistochemistry

Mouse spines were dissected and fixed in PBS 4% paraformaldehyde solution followed by decalcification in 20% EDTA pH 7.4. Decalcified tissues were processed and embedded in paraffin. Frontally embedded lumbar spine paraffin blocks were sectioned on a microtome to 5 µm thickness, 3-4 sections per slide. Each block yielded 40-50 slides. Every 5th slide was stained with Saffranin O and the sections were examined for the presence of disc degeneration. H&E, picrosirius red and Safranin O staining were performed according to standard protocols. Safranin O stained sections were imaged using Zeiss Observer D1 Axiocam 105 color camera and measurements of disc height and growth plate thickness were performed in ImageJ. Picrosirius red stained slides were imaged under brightfield or polarized light. The latter allows us to incorporate the birefringent properties of fibrillar collagen, in order to visualize the more organized collagen molecules.

IHC was performed using DAB staining method as described previously.[25] Briefly, the slides were deparaffinised and rehydrated. Antigen retrieval was performed using 1mg/mL Trypsin in PBS (Sigma) digestion for 10 min. Slides were washed and blocked with blocking solution (3% donkey serum in PBS TritonX 0.1%) for 1 h at room temperature. The slides were then incubated with primary antibody diluted in blocking solution overnight at 4°C. Subsequently slides were washed and incubated with fluorescent secondary antibody diluted in blocking solution for 1 h at 4°C. One of the sections on each slide was used as no primary antibody control.

Live imaging of p65-DsRed

Intervertebral discs from p65-DsRed mouse were cut in half to expose both the AF and NP tissue and embedded in the Matrigel matrix (BD Biosciences) in 35-mm glass bottom

Cellview dishes (Greiner Bio-one). Images were acquired with a Zeiss LSM 780 Confocal Inverted Microscope in a humidified CO_2 incubator (at 37°C, 5% CO_2) with a C-Apochromat 40×/1.2 W Korr objective. During imaging tissue was treated with IL-1β (5–20 ng/mL) or TNFα (up to 40 ng/mL). DsRedXP tagged p65 was visualized by excitation with a green helium neon laser (543 nm) and detection through both a 545-nm dichroic mirror and a 560-nm long pass filter. Data capture was performed using ZEN2010B software (Zeiss).

Statistical analysis

Data were evaluated using Two-tailed Student's *t*-test, two way ANOVA or non-parametric, two-tailed Mann-Whitney test. Results were presented as mean ± SEM from at least three independent experiments. Differences were considered significant at the values of *P < 0.05, **P < 0.01 and ***P < 0.001.